SANDIA REPORT
SAND2015-9786
Unlimited Release
Printed November 2015

Target Soil Impact Verification: Experimental Testing and *Kayenta* Constitutive Modeling

Scott T. Broome, Gregory M. Flint, Thomas Dewers and Pania Newell

Prepared by
Sandia National Laboratories
Albuquerque, New Mexico 87185 and Livermore, California 94550

Sandia National Laboratories is a multi-program laboratory managed and operated by Sandia Corporation, a wholly owned subsidiary of Lockheed Martin Corporation, for the U.S. Department of Energy's National Nuclear Security Administration under contract DE-AC04-94AL85000.

Issued by Sandia National Laboratories, operated for the United States Department of Energy by Sandia Corporation.

Available to DOE and DOE contractors from
U.S. Department of Energy
Office of Scientific and Technical Information
P.O. Box 62
Oak Ridge, TN 37831

Telephone: (865) 576-8401
Facsimile: (865) 576-5728
E-Mail: reports@adonis.osti.gov
Online ordering: http://www.osti.gov/bridge

Available to the public from
U.S. Department of Commerce
National Technical Information Service
5285 Port Royal Rd.
Springfield, VA 22161

Telephone: (800) 553-6847
Facsimile: (703) 605-6900
E-Mail: orders@ntis.fedworld.gov
Online order: http://www.ntis.gov/help/ordermethods.asp?loc=7-4-0#online

SAND2015-9786
Unlimited Release
Printed November 2015

Target Soil Impact Verification: Experimental Testing and Kayenta Constitutive Modeling

Scott T. Broome[1], Gregory M. Flint[1], Pania Newell[2], and Thomas A. Dewers[1]

[1]Geomechanics Department
and
[2]Solid Mechanics Department

Sandia National Laboratories
P.O. Box 5800
Albuquerque, NM 87185-0751

Abstract

This report details experimental testing and constitutive modeling of sandy soil deformation under quasi-static conditions. This is driven by the need to understand constitutive response of soil to target/component behavior upon impact. An experimental and constitutive modeling program was followed to determine elastic-plastic properties and a compressional failure envelope of dry soil. One hydrostatic, one unconfined compressive stress (UCS), nine axisymmetric compression (ACS), and one uniaxial strain (US) test were conducted at room temperature. Elastic moduli, assuming isotropy, are determined from unload/reload loops and final unloading for all tests pre-failure and increase monotonically with mean stress. Very little modulus degradation was discernable from elastic results even when exposed to mean stresses above 200 MPa. The failure envelope and initial yield surface were determined from peak stresses and observed onset of plastic yielding from all test results. Soil elasto-plastic behavior is described using the Brannon et al. (2009) *Kayenta* constitutive model. As a validation exercise, the ACS-parameterized *Kayenta* model is used to predict response of the soil material under uniaxial strain loading. The resulting parameterized and validated *Kayenta* model is of high quality and suitable for modeling sandy soil deformation under a range of conditions, including that for impact prediction.

Acknowledgments

The authors would like to thank Steve Bauer and Moo Lee for their critical review of this report. Funding from B-61 group is gratefully acknowledged. Sandia National Laboratories is a multi-program laboratory managed and operated by Sandia Corporation, a wholly owned subsidiary of Lockheed Martin Corporation, for the U.S. Department of Energy's National Nuclear Security Administration under contract DE-AC04-94AL85000.

Contents

Figures

Tables

Table 1

1. Introduction

This report summarizes an experimental testing and modeling effort performed in response to a need by B61-12 team members to characterize mechanical properties of a sandy soil. This is in support of future testing and subsequent fielding of B61-12 impact verification. To carry out this program, a test matrix is developed covering the range of 0 to 100 MPa confining pressure and expected differential stresses ranging from near zero to over 275 MPa (the latter estimated from literature sources). A key undetermined factor in development of the test matrix was prediction of potential compaction magnitudes with instrumentation operating over a wide range of stress and strain yet with the precision required to determine elastic properties and plastic response. A portion of this testing matrix was carried out in a series of UCS, ACS, hydrostatic, and uniaxial strain experiments at Sandia's Geomechanics Laboratory. Results of the elastic and plastic responses were used to develop a parameterized and validated model *Kayenta* (Brannon et al., 2009) that can be used for subsequent finite element predictions of material response over the quoted conditions.

2. Methods

2.1 Experimental Testing Design

A large quantity of prepared sandy "soil" was obtained from a locality near San Ysidro, New Mexico. This soil is composed of a mixture of two soils that was found to be an excellent base for making adobe blocks for building materials. This material was sieved to remove coarse particles > 2.8 mm (using a number 7 sieve). Particle size analysis was performed by a combined wet sieve and hydrometer ASTM method by Daniel B. Stephens and Associates, Inc. of Albuquerque, NM (see Appendix C for the detailed report) and was found to be composed of 56.9 % sand (greater than 0.075 mm and less than 4.75 mm), 30.2 % silt (greater than 0.002 mm and less than 0.075 mm), and 13.0 % clay (less than 0.002 mm). As such this material is classifiable as a silty sand (ASTM) or sandy loam (USDA). Compositionally the material is a mixture of decomposed granite and basaltic material; no mineralogical assay was performed.

This material was configured into a right cylinder nominally 2.0 inches in diameter and 4 inches in length by means of a TFE Teflon roll cover jacket that had been heat-shrunk over a cylindrical mold. Samples were initially tested in two configurations, "gravity pour", in which the material was simply poured into the Teflon jacket, and "tamped", in which the material after pouring was gently tapped in 3 to 5 lifts to a pre-determined density. The complete designed experimental matrix and all raw data of completed tests are given in Appendix A. **Table A-1** is partially populated and represents tests completed to date (ten hydrostatic, nine ASC and one uniaxial strain).

Samples were instrumented with a lateral deformation gage for radial displacement and two +/- 2.5 cm range Linear Variable Differential Transformers (LVDT's) for axial displacement measurements. The lateral and axial deformation gages were selected to provide enough resolution for accurate elastic modulus calculations while having enough range to track the large amount of expected sample compaction during hydrostatic and triaxial compression as well as radial expansion accompanying dilatation as localized failure was approached. Figure 1 shows an example of an instrumented specimen. **Figure 2** shows an example of the computer-controlled

servo-hydraulic testing system used to conduct the compression tests at ambient temperature. The system consists of an MTS reaction load frame, coupled with an SBEL (Structural Behavior Engineering Laboratory) pressure vessel rated to 15,000 psi (100 MPa). The pressure vessel housing the test specimen was connected to a pressure intensifier capable of inducing pressures up to 30,000 psi (200 MPa). Isopar® is used as the confining medium. The reaction frame has a movable crosshead to accommodate pressure vessels of different sizes and configurations. The frame used is capable of applying loads up to 220,000 pounds (1 MN) through a hydraulic actuator in the base of the frame. Vessel pressures were measured with a pressure transducer plumbed directly into the hardline that connects the pressure vessel to the pressure intensifier. The transducer is located about 5 ft (0.15 m) from the pressure vessel. Axial forces were measured with a load cell attached to the reaction frame outside of the pressure vessel (shown in **Figure 2**).

Results for all tests include axial stress, confining pressure, and axial and lateral displacement. Stresses and strains are reported as "true" values which account for sample geometry changes. True strain is defined as the natural logarithm of the current length divided by the initial length; in the case of lateral and volume strain, the natural logarithm of current diameter and volume are divided by the corresponding initial values. True strain is well suited when measuring large strains (typically over 2%) but are essentially equal to engineering strains at lower values.

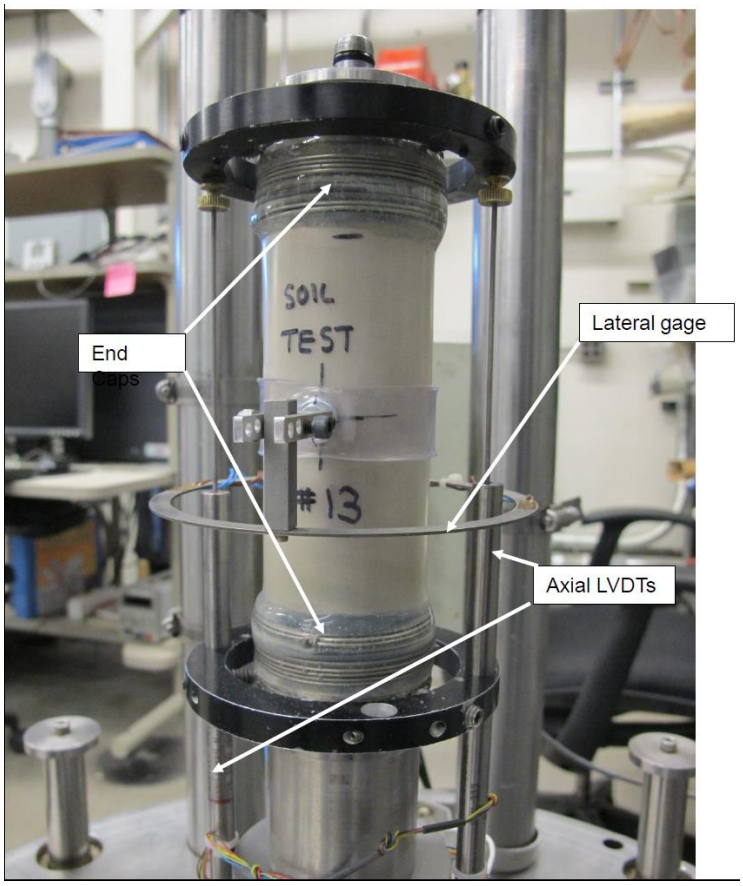

Figure 1. Instrumented sample mounted on the 100 MPa pressure vessel base.

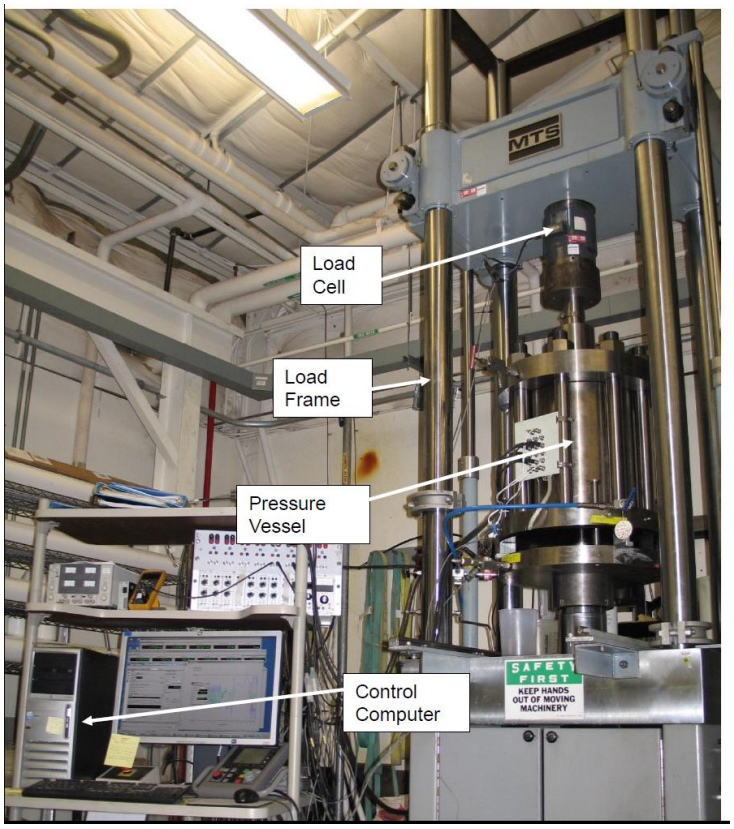

Figure 2. 220,000 lb (1 MN) load frame with 15,000 psi (100 MPa) pressure vessel. Data acquisition system is show to the left of the load frame.

2.2 Constitutive Modeling

To model the observed elastic-plastic constitutive behavior of the tested soil, we apply the *Kayenta* generalized plasticity model described by Brannon et al. (2009). *Kayenta* is based on work by Schwer and Murray (1994) in that it links a shear yield surface to a Pelessone (1989) function to generate a single smoothly differentiable yield surface including a "cap" at higher mean stresses, applicable to pore collapse. Unique hardening functions are used to quantify the competition between dilatation from micro-cracking and compaction from pore collapse. *Kayenta* employs a general failure surface that can be tailored to capture Coulomb or other observed failure types. As a constitutive model, *Kayenta* has been extensively verified (documented on pages 102 to 112, Brannon et al., 2009) and validated (described on pages 121 to 124, Brannon et al., 2009). Details on the mathematical and computational formulations are given in Brannon et al. (2009); earlier versions of the model are described by Fossum and Fredrich (2000) and Foster et al. (2005). These authors detail improvements of the approaches utilized in *Kayenta* over other cap plasticity and critical state soil mechanics models. These include, but are not limited to, the following features:

• Three-invariant, mixed hardening, non-associative plasticity.

• Nonlinear (stress dependent) elasticity.

• Nonlinear peak shear failure threshold for fully damaged material.

• Kinematic hardening.

• Nonlinear compaction function (pressure-volume) with isotropic hardening.

Kayenta was used previously to model elasto-plastic constitutive response of weak porous sandstone in Dewers et al. (2014). Here our purpose is application and parameterization of *Kayenta*, and comparison to experimental results on sandy-soil deformation via a single-element material driver, which are described in a later section.

3. Results

3.1 Experimental Results and Discussion

Load paths for all tests used in *Kayenta* parameterization are shown in Figure 3. Not shown are the single hydrostatic test (#11-1) or the uniaxial test (#2), which will be discussed later. Initial porosity, load paths, and peak stress invariants for these tests are given in Table .

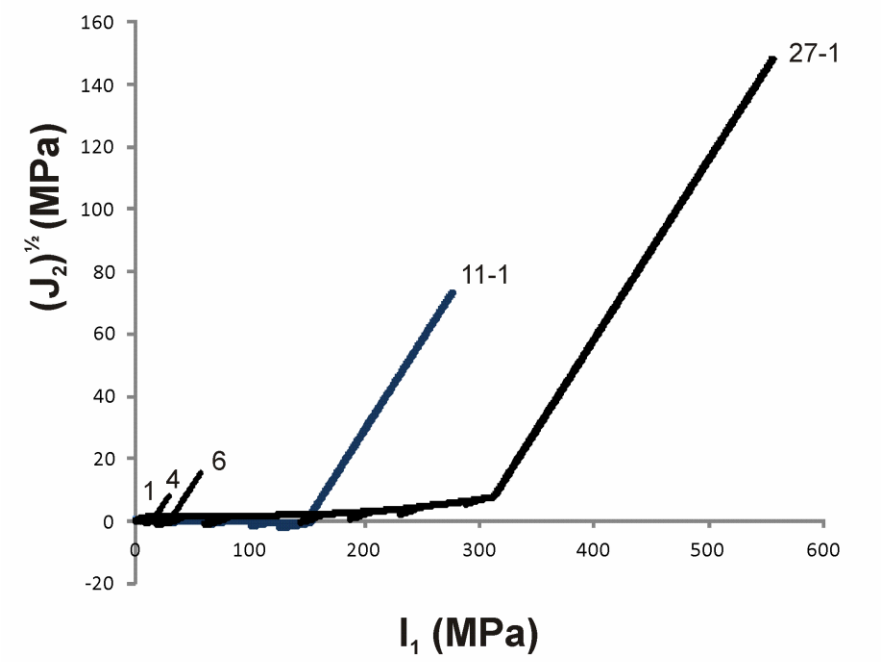

Figure 3. Load paths for USC and ASC tests. Tests 3 and 5 are duplicates for 4 and 6 respectively and are not shown for clarity.

Peak stresses are reported in Table in terms of the first (I_1) and second ($J_2^{1/2}$) stress tensor invariants. For our experimental configuration, these are simply defined as

$$I_1 = 3\sigma = \sigma_A + 2\sigma_L \qquad (1A)$$
$$(J_2)^{1/2} = \tau = (\sigma_A - \sigma_L)/\sqrt{3} \qquad (1B)$$

where σ is mean stress, τ is the signed equivalent shear stress or Von Mises shear stress, and the subscripts 'A' and 'L' refer to axial and lateral respectively. Our sign convention used here is that compressive stresses and strains are positive as is common for experimental data reporting in the geomechanics literature. Note that *Kayenta* uses the opposite sign convention but we report results to be consistent with this choice. Similarly volume (ε) and shear strains (γ) are defined as

$$\varepsilon = \varepsilon_A + 2\varepsilon_L \qquad (2A)$$
$$\gamma = 2(\varepsilon_A - \varepsilon_L)/\sqrt{3} \qquad (2B)$$

Table 1. Tests examined for constitutive behavior and *Kayenta* modeling.

Test #/Type	Initial Porosity	Confining P (MPa)	Peak $(J_2)^{1/2}$ (MPa)	Peak I_1 (MPa)
1/UCS	0.438	0.0	1.23	0.71
2/Uniaxial strain	0.425			
3/ASC	0.429	5.0	24.4	5.40
4/ASC	0.381	5.0	29.5	8.34
5/ASC	0.458	10.0	55.8	14.9
6/ASC	0.429	10.0	57.3	15.7
11-1/hydrostatic	0.435			
11-2/ASC	0.350	50.0	276	73.0
27-1/ASC	0.350	100.0	556	148

Axial stress plotted versus axial and lateral strain data are given up to peak stress for all relevant tests in **Figure 4**. Note multiple unload/reload loops performed during both hydrostatic and shear stress paths. Unload/reload loops are used to determine bulk and shear moduli (assuming that the soil material is elastically isotropic) as a function of material parameters and represent the elastic component of the elastic/plastic pressure curve.

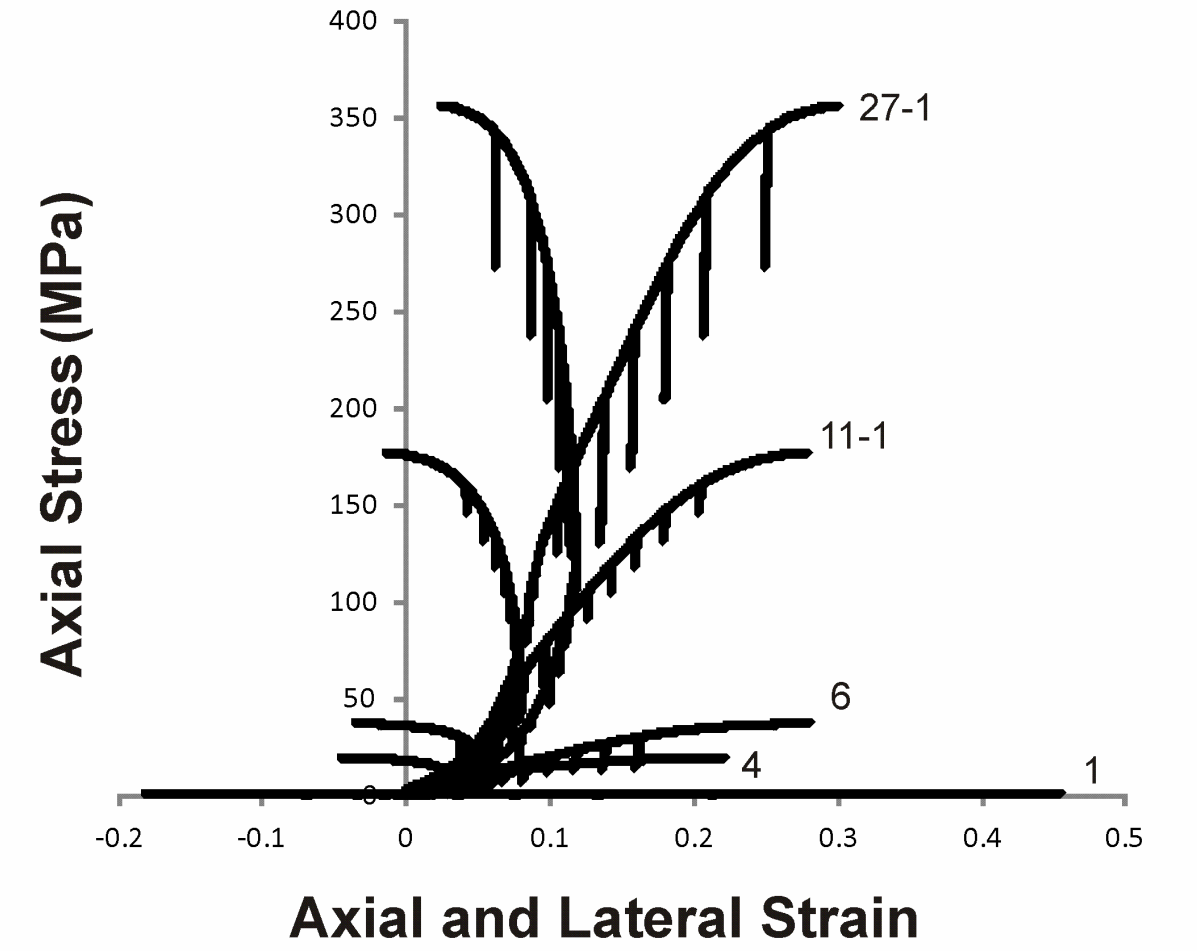

Figure 4. Axial (right) and lateral (left) strains for UCS and ASC tests. Tests 3 and 5 are duplicates for 4 and 6 respectively and are not shown for clarity. The UCS test results are barely discernable in the figure.

During unloading loops, stress and strain exhibit hysteresis as a result of the use of an external load cell. Friction between piston and piston seal (where the piston enters the pressure vessel) delays transmission of load from the loading system to the sample, both on unloading and reloading. To surmount this, only portions of unloading loops, wherein friction has been overcome, were used to infer elastic properties during plastic yielding. This is discussed further below. Pre-peak stresses and strains were used in determining elastic moduli evolution, as after peak (corresponding to shear or compaction localization) the soil specimens can no longer be considered as nominally homogeneous.

Figure 5 shows example hydrostatic loading from tests #6, 11-2, 11-1, and 27-1. Test 11-1 was ended prior to failure and so the final unload loop, showing unloading from ~50 MPa to 0 MPa is reflective of the elastic behavior of the homogeneous material. The slopes of the unload loops in **Figure 5** are equivalent to the tangent bulk moduli, which is seen to behave nonlinearly with mean stress. It is evident from the departure of the unload loops from the loading curves that plastic deformation commences almost immediately with application of load. The differences in the hydrostats among these tests shown in **Figure 5** are due to the differences in starting volume

strain (or initial porosity). Test 11-2 is a continuation of 11-1; Test 27-1 is a "tamped" sample. Both of these initiate with a lower bulk density or lower initial porosity (~0.35) compared to the gravity pour samples #11-1 and #6 which experienced no prior loading. All gravity pour samples have hydrostatic loading curves similar to these latter tests but are not shown for clarity.

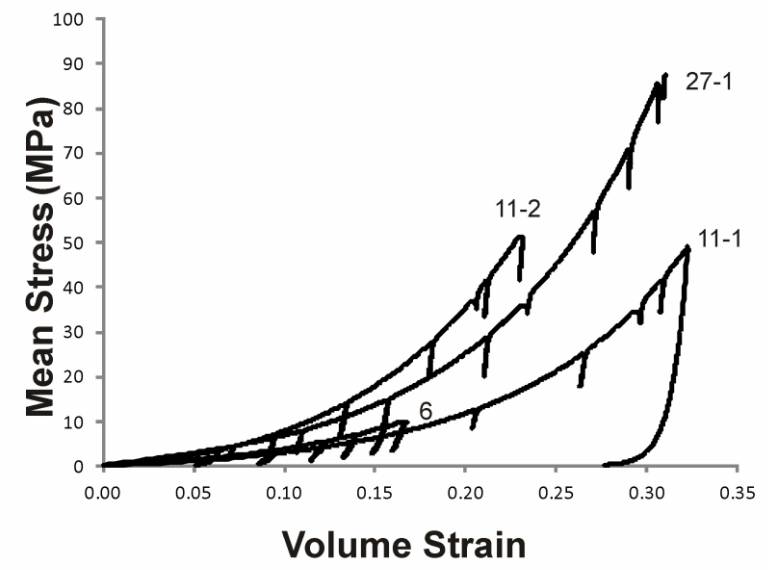

Figure 5. Hydrostatic loading paths for selected tests, showing variability in plastic loading among experiments. Test 11-1 shows complete final unloading and as this test was run to a pre-failure peak stress, these results are used to suggest a form of the mean stress dependence of the secant and tangent bulk modulus.

3.2 Nonlinear elasticity

Initial loading up to yield, and unloading curves for all load paths display a nonlinear elastic behavior. With an assumption of isotropy, these can be quantified by a stress-dependent bulk and shear modulus (*K* and *G* respectively).

In this treatment, we follow Dewers et al. (2014) and assume an elastic strain that follows from

$$\sigma_{ij} = C_{ijkl}\varepsilon^{e}_{kl} \qquad (3)$$

which, with assumptions of isotropy and using the definitions in equations (1) and (2), becomes

$$\varepsilon^{e} = \frac{\sigma}{K}, \quad \gamma^{e} = \frac{\tau}{G} \qquad (4A)$$

Here and in following equations, a superscript 'e' is used to refer to elastic strains in order to differentiate from plastic strains, using the superscript 'p'. For nonlinear elasticity, the moduli in (4A) are termed "secant" moduli, distinguished from local slopes of stress-strain curves, which are termed "tangent" moduli. These would be found from incremental theory as (the subscript 'tan' refers to tangent moduli; moduli with no subscripts refer to secant moduli)

$$d\sigma = K_{\tan} d\varepsilon^e \quad \text{and} \quad d\tau = G_{\tan} d\gamma^e \qquad (4B)$$

From an assessment of experimental behavior, following Dewers et al. (2014), we have made the following parameterization in which *K* and *G* depend on mean stress. Mathematical forms we have found to fit complete unloading curves to an excellent degree, for *K* and *G*, here noted as secant moduli, are given as:

$$K = K_0\left(1 + K_1\sigma - K_2 e^{-K_3\sigma}\right) \qquad (5A)$$

$$G = G_0\left(1 + G_1\sigma - G_2 e^{-G_3\sigma}\right) \qquad (5B)$$

The form of these equations is suggested from work on p- and s-wave velocities in weak porous sandstones and we apply them here to unconsolidated sandy soil. Kaselow and Shapiro (2004) give a theoretical basis for this stress dependence in which the exponential portion in (5A) derives from compliant microcracks and crack-shaped pores, and the linear portion derives from more rounded pores. The linear term in σ in (5A) is a common form in critical state soil mechanics as well. The form of mean stress dependence of the shear modulus in (5B) is different from that applied by previous authors (e.g. Hueckel et al. (1992) and Jeske and Lefik (2005) favor a square root dependence on mean stress; however the exponential term in 5B yields nearly identical behavior at low mean stresses). Eqns (5) are shown below to be applicable over the entire mean stress range applied in these tests. To determine the (5A) K_i and (5B) G_i constants, we have found it to be a more convenient and accurate determination to fit the full stress-strain behavior during elastic unloading portions using the secant moduli (i.e. in 4). In our constitutive modeling with *Kayenta*, we use tangent moduli which are convenient for incremental elastic-plastic theoretical treatments. For the bulk modulus, the tangent bulk modulus K_{tan} can be found from the secant modulus *K* in (5A) via the slope of the stress strain curve as

$$K_{\tan} = \left\{\frac{1}{K} - \frac{\sigma}{K^2}\left(K_0K_1 + K_0K_2K_3e^{-K_3\sigma}\right)\right\}^{-1} \qquad (6A)$$

Similarly, we use

$$G_{\tan} = \left\{\frac{1}{G} - \frac{\sigma}{G^2}\left(G_0G_1 + G_0G_2G_3e^{-G_3\sigma}\right)\right\}^{-1} \qquad (6B)$$

For unloading curves, when combined with (4A), Equations (5A and B) give an excellent fit to experimental data. For example, in Fig. 6, taken from the hydrostatic test 11-1, the final unloading data (dotted line) are well described by a bulk modulus parameterized by {K_0, K_1, K_2, K_3} = {1148.0 MPa, 0.0098 MPa^{-1}, 0.93 MPa^{-1}, 0.012} as shown by the dashed line.

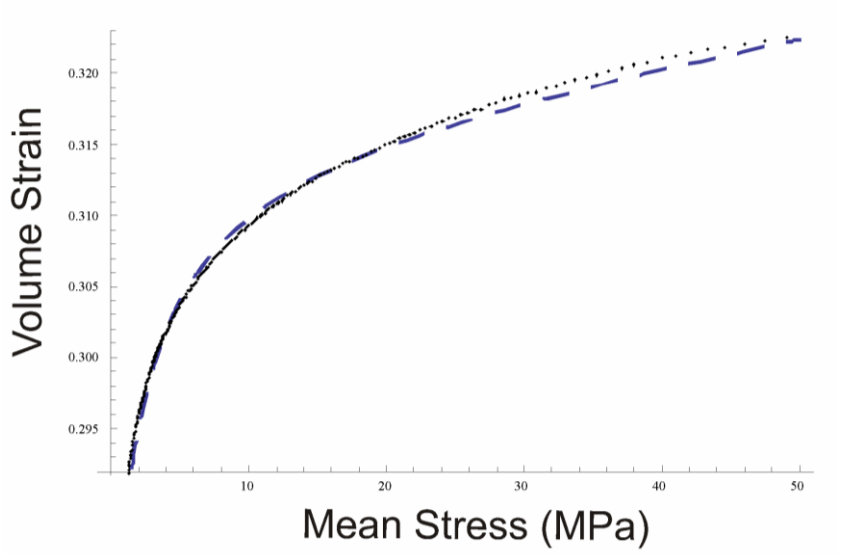

Figure 6. Fit of final unloading curve of test 11-1 to proposed nonlinear bulk modulus relation given in Eqn 5A. The best fit relation is shown by the dashed line with {K_1, K_2, K_3, K_4} = {1148.0 MPa, 0.0098 MPa^{-1}, 0.93 MPa^{-1}, 0.012}; data is shown as points.

Curve fitting for moduli make use of the following expressions, valid for the elastic portions of the respective stress-strain curves (Dewers et al., 2014):

$$\varepsilon^e_{\max} + \varepsilon^p = \varepsilon^p + \varepsilon^e_{\min} + \frac{\sigma_{\max}}{K(\sigma_{\max})} - \frac{\sigma_{\min}}{K(\sigma_{\min})} \qquad (7A)$$

$$\gamma^e_{\max} + \gamma^p = \gamma^p + \gamma^e_{\min} + \frac{\sigma_{\max}}{G(\tau_{\max})} - \frac{\sigma_{\min}}{G(\tau_{\min})} \qquad (7B)$$

We have applied this procedure to all stress-strain data. In the case of uniaxial and non-hydrostatic portions of the triaxial tests, we fit the axial stress-strain data to determine Young's Modulus, E, and then find the shear modulus from the following expression, using expressions in (5) and the bulk modulus determined from the hydrostatic loading portions:

$$E = \frac{9KG}{3K + G} \qquad (8)$$

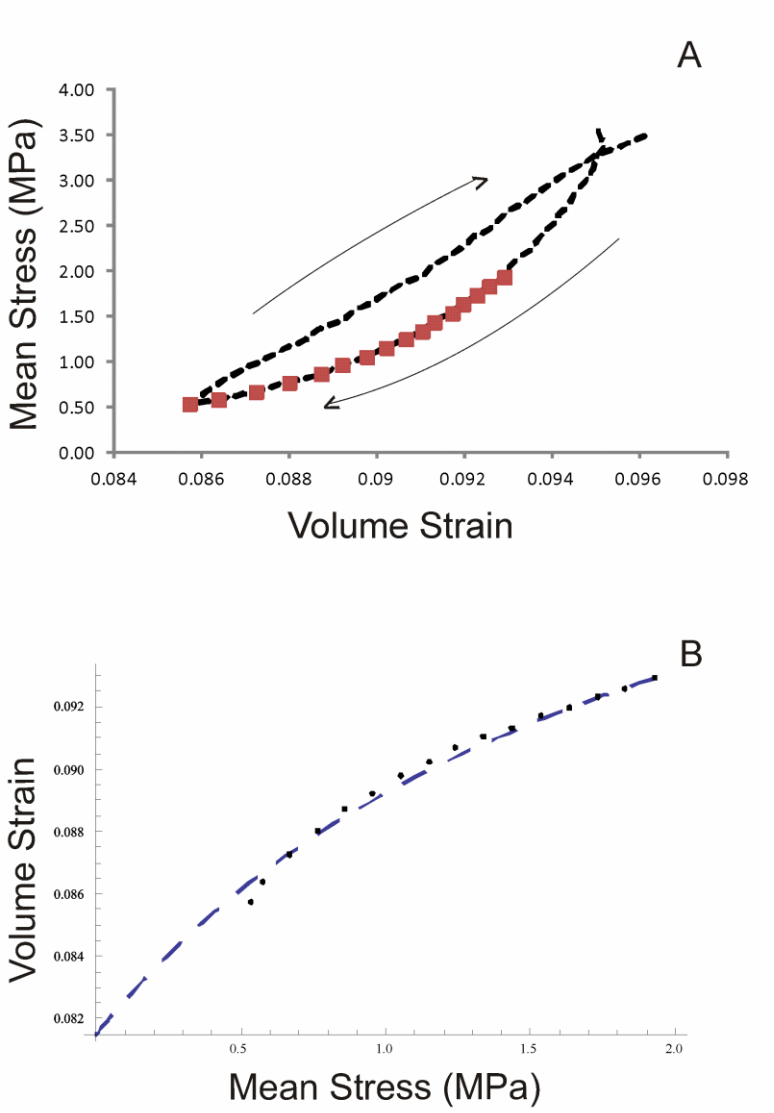

Figure 7. A. Example of a unload-reload loop from test #6, under hydrostatic unloading (this is the second loop in the series). The square symbols delineate the portion of the loop used to determine secant bulk moduli. B. Dashed line shows curve fit of data in A. (shown as dots) to eqn 7A, which gives $\{K_1, K_2, K_3, K_4\}$ = {1200 MPa, 0.005, 0.9766, .0120}.

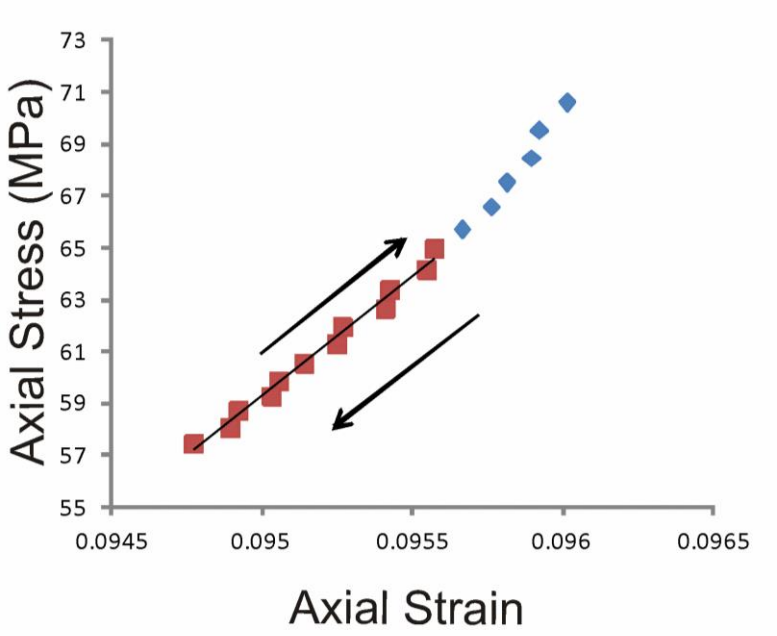

Figure 8. Unload-reload loop in the space of axial stress versus axial strain (loop eight in the sequence with increasing strain) from test 11-2. The straight line shows linear fit of tangent Young's modulus, which in turn is used to calculate tangent shear modulus using eqn. 8. Best fit from linear regression yields an E_{tan} = 9228.0 MPa with R^2 = 0.989.

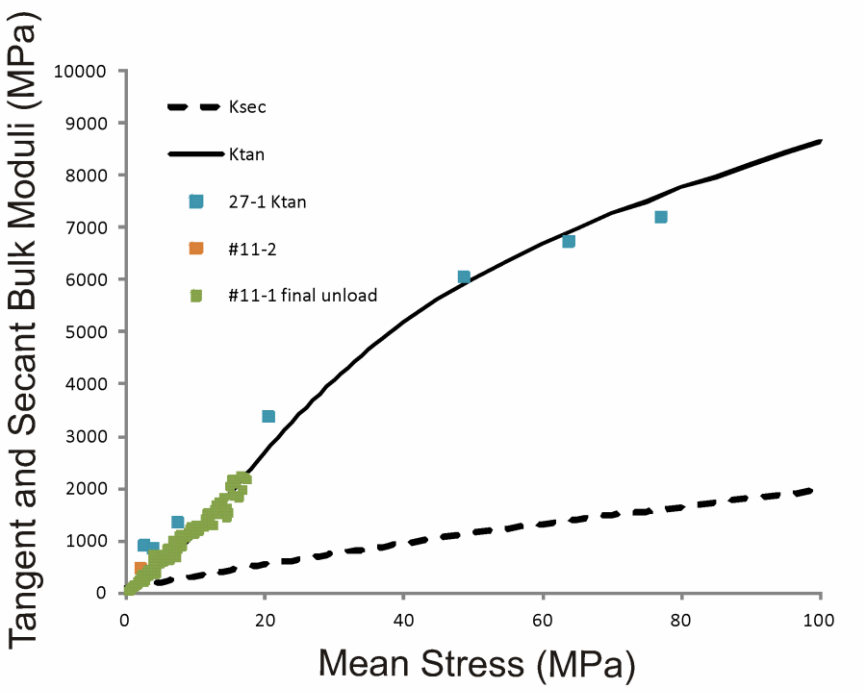

Figure 9. Secant (dashed line) and tangent (solid line) bulk modulus determined from global fit to Eqn 6A, which yields {K_1, K_2, K_3, K_4} = {1148 MPa, 0.0098, 0.93, 0.012}, which are slightly different from those shown in **Figure 5** and **Figure 6.**

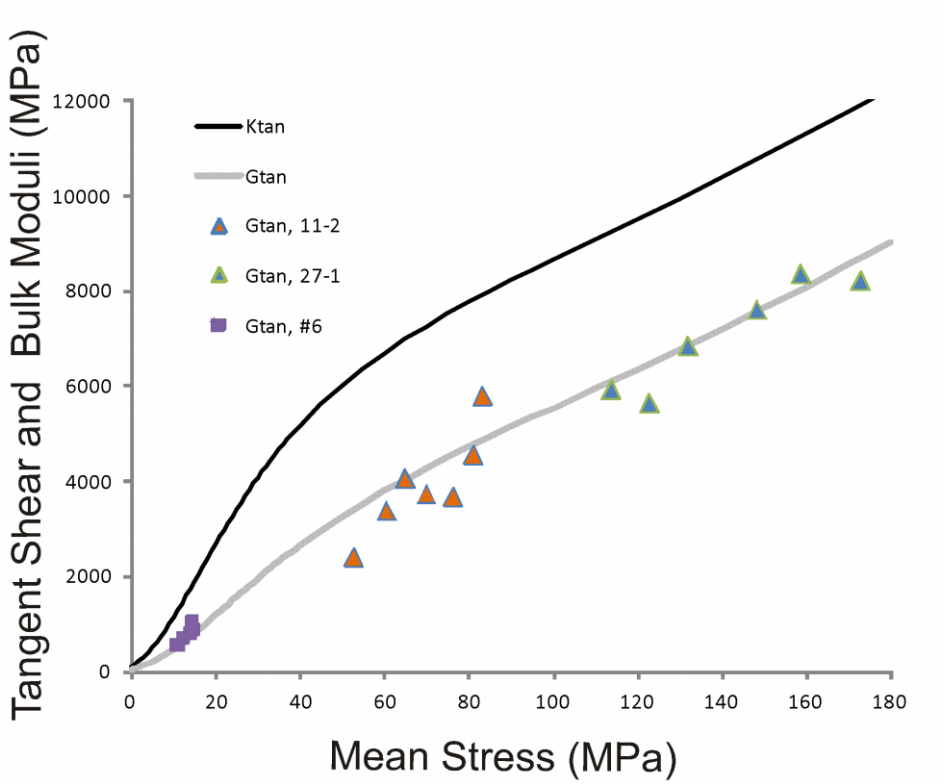

Figure 10. Best fit tangent shear modulus (grey line) from Eqn 6B, determined from tangent Young's modulus (as demonstrated in **Figure 8**) and tangent bulk modulus (shown as black line; same as in **Figure 9**). Data points are tangent shear modulus values determined from unload loops in the individual experiments. The parameters for the tangent shear modulus shown by the grey line are $\{G_1, G_2, G_3, G_4\}$ = {300 MPa, .020, 0.90, 0.012}.

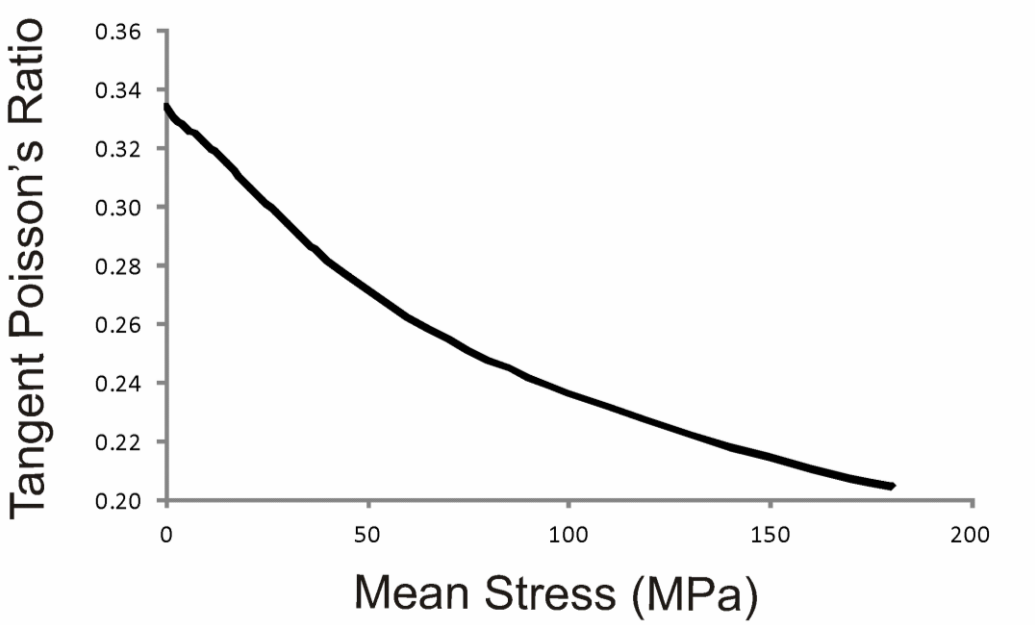

Figure 11. Tangent Poisson's ratio determined from tangent bulk and shear moduli given as solid lines in **Figure 10**.

For simplicity, in cases where there is a clear plastic strain dependence of elastic moduli as revealed via the unloading cycles or final unloading, we assume that the moduli depend only on the conjugate plastic strains, so that, for our purposes here,

$$K = K(\sigma, \varepsilon_p) \qquad (9A)$$

$$G = G(\sigma, \gamma_p) \qquad (9B)$$

In examining moduli values for unload loops through all experiments however, we have found that very little modulus degradation is evident. We subsequently ignore modulus degradation, which greatly simplifies the *Kayenta* modeling shown later.

3.3 Strain Separation

To partition total strains into elastic and plastic strains, we start with common assumptions in elastic-plastic constitutive models, namely the additive nature of elastic and plastic parts

$$\varepsilon_{ij}^{t} = \varepsilon_{ij}^{e} + \varepsilon_{ij}^{p} \qquad (10)$$

Plastic strain can then can be found from (10) by subtracting the calculated elastic strain, found from the modulus-mean stress relations and eqns (4A), from the total strain. This is shown for the hydrostatic test #11-1 in Figure 16.

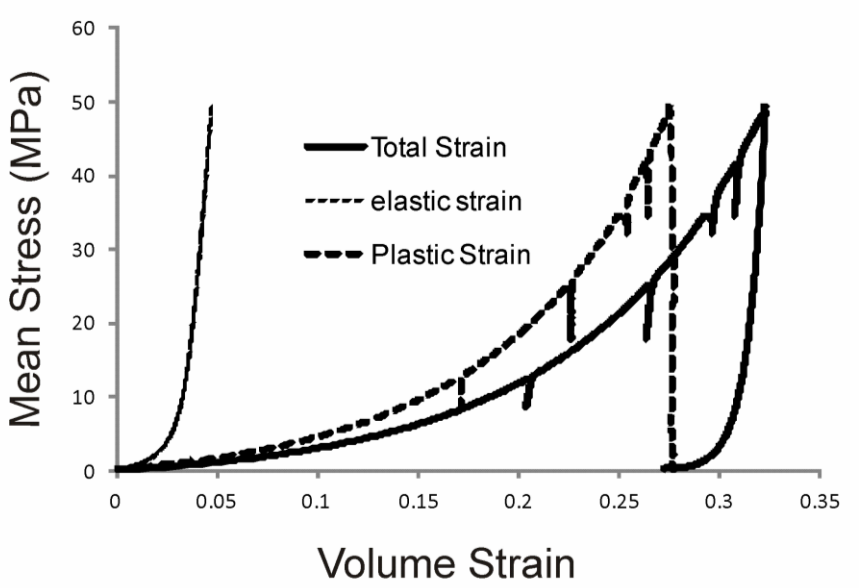

Figure 12. Hydrostat data from test 11-1 (solid line) separated into elastic (dotted line) and plastic (dashed line) portions, using the secant bulk modulus relation shown in **Figure 6.**

3.4 Initial Yield and Failure Envelopes

In this section we apply the observed peak stresses listed in Table and observed initial yield stresses to models for failure and yield envelopes as per the *Kayenta* theory (Brannon et al., 2009]. In accord with plasticity theory *Kayenta* defines a yield function *f* in stress space such that elastic states satisfy $f < 0$. *Kayenta* uses a single, continuously differentiable function to define a single yield surface that accounts for the yielding effects of microcracking and dilatation as well as the effects of pore collapse.

For the failure envelope, *Kayenta* uses the function

$$F_f(I_1) = a_1 - a_3 e^{-a_2 I_1} + a_4 I_1 \qquad (11)$$

which is general enough to be used for modeling a variety of observed shear-limit surfaces observed in real materials, including Mohr-Coulomb behavior. **Figure 13** shows the failure or limit surface (11) to be linear. We find with a full nonlinear regression with equation (11) that the experimental peak stresses follow a limit or failure surface with $\{a_1, a_2, a_3, a_4\} = \{0.95, 0.011, 0.585. 0.262\}$, but a simpler linear function with $\{a_1, a_2, a_3, a_4\} = \{0, 0, 0, 0.266\}$ fits the function with an R^2 coefficient of 0.999. This would imply that the soil material is essentially cohesionless, which is evident from inspection of the starting material.

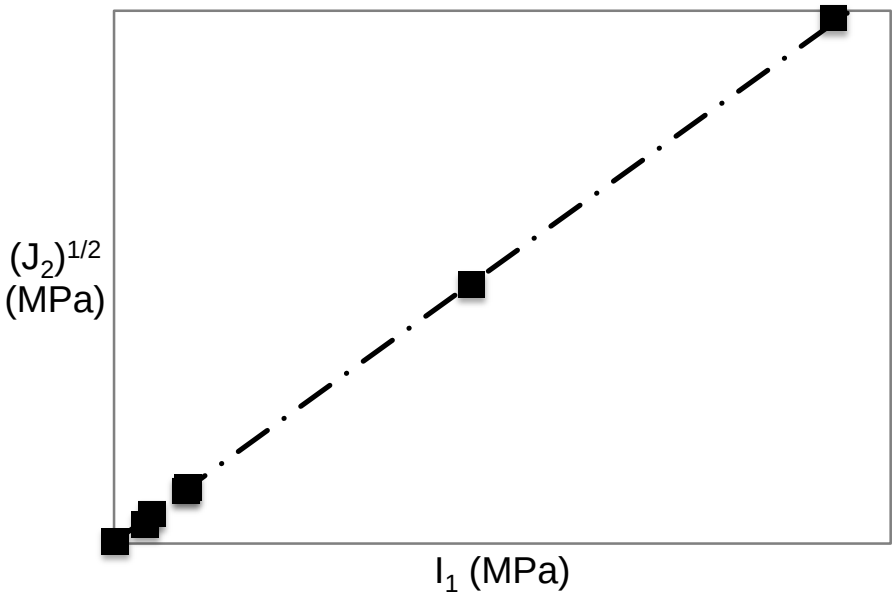

Figure 13. Failure surface determined from peak stresses from UCS and all ASC tests (Table) using the *Kayenta* expression from Brannon et al. (2009) given in Eqn 11. Best fit parameters are $\{a_1, a_2, a_3, a_4\} = \{0.95, 0.011, 0.585. 0.262\}$ although {0, 0, 0, 0.266} also describes the data nearly perfectly.

For the yield envelopes, *Kayenta* employs the following form

$$\sqrt{J_2} = \frac{f_f(I_1) f_c(I_1)}{\Gamma(\theta)} \qquad (12)$$

where

$$f_f(I_1) = F_f(I_1) - N \qquad (13)$$

and N is an offset parameter that can be used to model kinematic hardening effects. The details of how *Kayenta* models kinematic hardening are given in Brannon et al. (2009). The cap function f_c is modeled after the Pelessone (1989) function

$$f_c^2(I_1, \kappa) = 1 - \frac{(I_1 - \kappa)(|I_1 - \kappa| + (I_1 - \kappa))}{2(X - \kappa)^2} \qquad (14)$$

where κ is an internal state function used by *Kayenta* to track the isotropic hardening, or expansion of the yield envelope, with progressive plastic straining. X is the I_1 value at the intercept of the yield envelope with the hydrostat, and so marks the initiation of plastic yielding (pore collapse) with hydrostatic loading. The rate of change of κ is proportional to the rate of plastic volume straining, but we leave the details of this mapping to the discussion provided in Brannon et al. (2009). $\Gamma(\theta)$ in (12) is a term that depends on lode-angle θ, a function of the second and third principal invariants of the deviatoric stress tensor. As we only discuss axisymmetric testing results here, we lack the data sets to discuss lode-angle dependence, and so this function is set to unity. *Kayenta* has the capability of accounting for J_3 (i.e. the third stress invariant) dependencies on yield and failure and thus modeling geomaterial behavior under general subsurface stress states, but this is beyond the scope of our treatment.

In plasticity theory, the increment of plastic strain is equal to a multiplier, termed the consistency parameter, multiplied by the gradient of a flow potential with respect to stress (e.g. Brannon et al., 2009, their equation 4.54). For associative plasticity, the flow potential equals the yield surface or envelope and this has been found suitable for describing plastic flow in metals, where the direction of plastic yielding is normal to the yield envelope. For porous geomaterials on the other hand, associative plasticity tends to overpredict the plastic volume strain (Brannon et al., 2009), in that the direction of plastic yielding is not normal to the yield envelope. This has led workers to propose a different flow potential function not associated with the yield envelope, and this is termed non-associative plasticity. *Kayenta* allows for non-associative plasticity by defining the flow potential function similarly to the yield envelope but replacing the a_2 and a_4 parameters in equation (11) with the non-associative counterparts $a_{2,n}$ and $a_{4,n}$, as well as the κ in equation (14) with its non-associative counterpart κ_n. This results in a flow potential with a different shape than the yield envelopes in Figure 10, and thus the strain path upon yielding can be non-normal to the yield function (and thus the amount of dilatational volume strain can be much less than would be predicted by associative plasticity assumptions, for example). For the soil samples examined herein, non-associative plasticity is necessary to describe strain evolution for the triaxial tests, where yielding is near the apex of the yield envelope or on the "cap" but is not critical for modeling strain paths associated with UCS tests. This is explored further below.

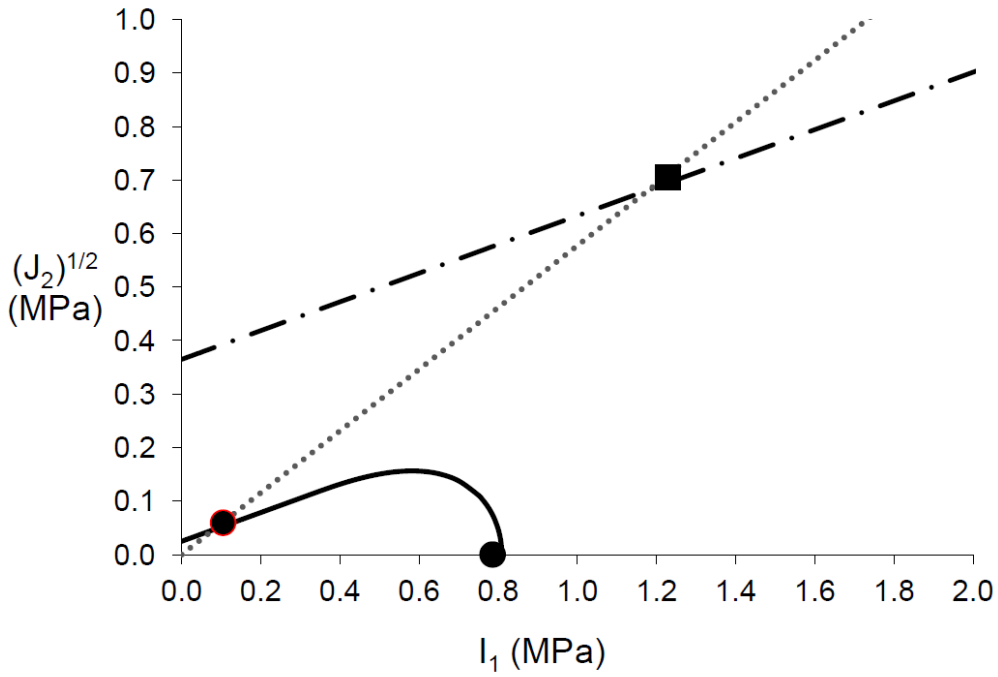

Figure 14. Initial yield surface (solid line), constrained by estimates of initial yielding from UCS and ACS tests, as given by eqns (12), 13), and (14). The intercept at the hydrostat at inception of yielding (X in eqn 14) is 0.8 MPa. The κ parameter in eqn 14 is found to 0.35 MPa. Yielding commences almost with initiation of load application in all tests. Failure surface is given by the dashed line, and constrains the level of kinematic hardening, with the 'N' parameter in eqn 13. equal to ~0.34 MPa.

3.5 "Crush-Curve" Parameterization

The evolution of plastic volume strain post-yielding used by *Kayenta* is modeled by a "crush-curve" function similar to that used by Gurson (1977), which tracks the plastic volume strain after the mean stress has exceeded a threshold value P_E (marking the onset of plastic yielding along the hydrostat):

$$\varepsilon_v^p = P_3\left(1 - e^{-(P_1 + P_2\xi)\xi}\right) \qquad (15A)$$

or, with rearranging;

$$-Ln(1 - \frac{\varepsilon_v^p}{P_3}) = (P_1 + P_2\xi)\xi \qquad (15B)$$

where $\xi = 3(\sigma - P_E)$. As P_E is a fraction of an MPa for the tested soil, for our purposes, $\xi \sim 3\sigma$ or approximately equal to I_1. The P_1 and P_2 values can be obtained by fitting the plastic volume strain determined in the previous section. P_3 is the logarithmic residual volume strain after full void collapse, and so is a function of initial porosity at the inception of loading. We find that curve fitting results are highly sensitive to the choice of P_3, which is related to the initial porosity (Brannon et al., 2009; p. 15) via

$$P_3 = \ln \frac{1}{1-\varphi_0} \qquad (16)$$

Figure 15 shows that, when proper accounting of initial porosity is made, plastic volume strain evolution from all experiments (with different hydrostatic loading paths, shown in **Figure 5**) can be well described by a single Gurson function. One limitation of the current *Kayenta* implementation, however, is the second-order polynomial function of mean stress in the exponential term in (15); the curve fit in **Figure 15A** (with fourth-order polynomial fit to 27-1 data) suggests that a more complex function is really required to describe the observed behavior. This would be a fruitful area of future *Kayenta* development and would improve the plastic volume strain modeling provided in the next section. A second order fit to the same data shown in **Figure 15B** doesn't describe the data as well; the second order fit in 15B has a maximum which could prove troublesome and not physical if this curve was used at higher mean stresses.

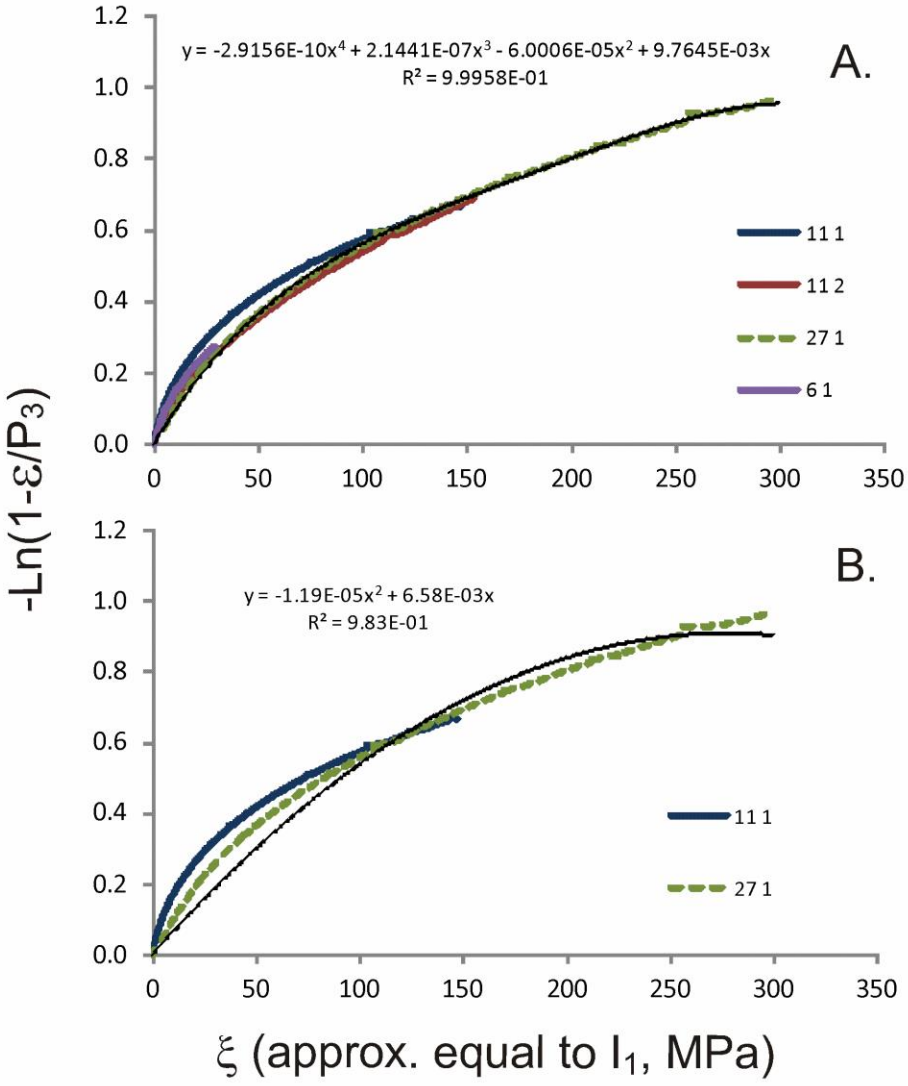

Figure 15. A. Equation 15B plotted using data from the calculated plastic strain curve for experiment 11-1(in Figure 12), as well as for that from experiments 11-2, 27-1, and 6-1. When using values of P_3 calculated from measured initial porosities using eqn 16, all plastic volume strain evolution tracks approximately along the same path. Values

of P_3 are: 0.56, 0.57, 0.37. and 0.43 for tests 6-1, 11-1, 11-2, and 27-1 respectively. The trendline (solid black) and resulting fourth-order polynomial fit (with R^2 essentially of unity) are fit using data from 27-1. **B**. Second order fit to experiment 27-1; the resulting '*P*' parameters are {*P1, P2*} = {6.58e-3; -1.19e-5} in MPa units.

3.6 Results of *Kayenta* Constitutive Modeling

In this section, experimental results are used in *Kayenta* elasto-plastic constitutive material model driver (*MatModLab*, authored by Tim Fuller, Sandia *Git* Repository) was run *Kayenta* on a single element. The stress paths used for the separate experiments cluster at low mean stresses, with two experiments provided to describe behavior at high stresses compared to seven experiments at lower mean stresses. Therefore, it was two sets of parameters; one for the low stress region, termed *local parameters;* and one entire stress region, using all of the data, termed *global parameters*. Elastic parameters (5) used for the *Kayenta* model runs are summarized in

Table 2, *P* parameters are given in Table 3 and non-associative potential function parameters are given in Table. All parameters are reported in units of Pa, which *Kayenta* uses, rather than the MPa used previously.

Table 2. Parameters for elastic moduli of all tests.

	K_0 (Pa)	K_1 (1/Pa)	K_2 (1)	K_3 (1/Pa)	G_0 (Pa)	G_1 (1/Pa)	G_2 (1)	G_3 (1/Pa)
Global	1148.00E+6	9.80E-9	0.93	0.012	300E+6	2.00E-8	0.9	0.012E-6
Local	1148.00E+6	9.80E-9	0.93	0.012	300E+6	2.00E-8	0.9	0.012E-6

Table 3. '*P*' parameters for (local) and (global) fits.

	P_0 (Pa)	P_1 (1/Pa)	P_2 (1/Pa^2)	P_3 (1)
Local	-0.78557	8.9E-9	-3.0E-17	0.571
Global	-0.78557	5.36E-9	-6.7E-18	0.371

Table 4. Non-Associative potential function parameters for (local) and (global) fits.

	HC (Pa)	CFPF (1)	A2PF (1/Pa)	A4PF (1)
Local	8.0E+2	1.629	0.011E-8	0.2423
Global	-0.78557	5.36E-9	-6.7E-18	0.371

Parameters describing the failure surface and yield function are given in **Figure 13** and **14** respectively. A complete set of parameters for use in direct input into *Kayenta* is given Appendix B.

3.6.1 Hydrostat Behavior

Combining the bulk modulus parameterization with the crush curve formalism discussed in the previous section provides a model for total volume strain with increase in mean stress, i.e. along the "hydrostat" with shear stresses equal to zero. **Figure 16** summarizes hydrostat behavior across a range of mean stress observed experimentally along with Kayenta simulated behavior.

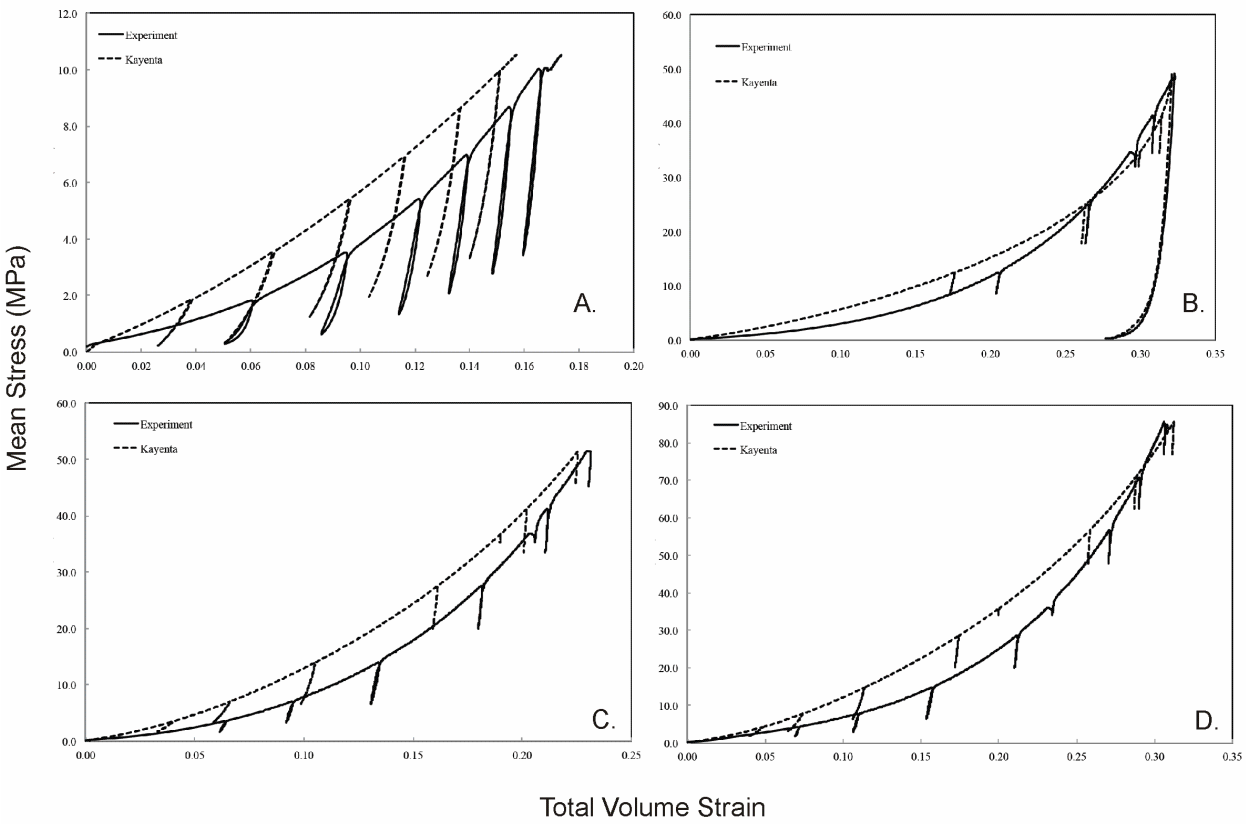

Figure 16. Hydrostatic test results shown in solid line together with Kayenta modeling results shown by the dashed curve. A. Experiment 6-1 B. Experiment 11-1, which shows a complete unloading. C. Experiment 11-2. D. Experiment 27-1.

11-1 is purely hydrostatic test that was completely unloaded to zero stress. The excellent match between experiment and modeling for the final unloading (and thus only elastic) portion in **Figure 16B** shows that the elastic model in Kayenta is an excellent description of experimental behavior, and that the discrepancy between total strain experimental and modeled curves during the loading portions is from the mismatch in the crush curve model. In general, the second-order polynomial fit used for the *Kayenta* model underestimates plastic volume strain compared to experiment.

3.6.2 Unconfined Compressive Stress Test 'UCS 1'

The testing results of the UCS test were used in determination of initial yielding, however the material, as essentially cohesionless sand, would not be expected to have an unconfined compressive strength. The behavior of the jacketed sand with no confining pressure, shown in Figure 17, is arguably that of a low-cohesion solid, but the stress-strain paths above ~ 1 MPa are arguably dominated by the jacket material itself undergoing yielding. As such, we have used the results of this test in an earlier section to constrain the mean stress dependence of Young's modulus at low mean stress, and to constrain the initial yielding (below 0.2 MPa axial stress, as indicated by the departure of the first unload loop from the loading curve), but we don't attempt Kayenta modeling.

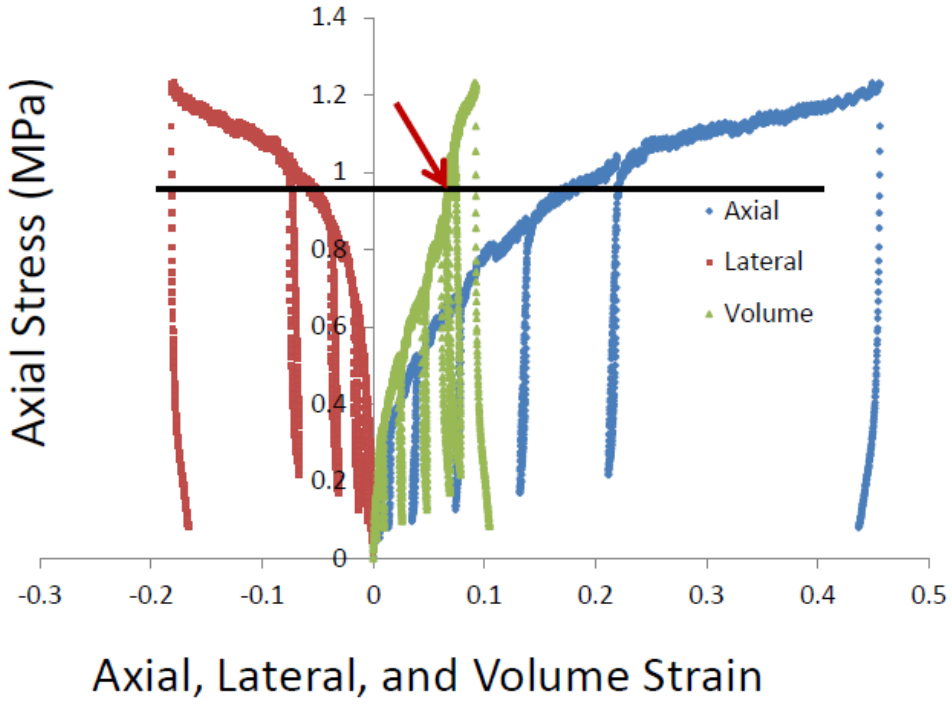

Figure 17 UCS test results modeling by *Kayenta*: The volume strain, shown in green, begins a "turn around" resulting from a shift from compression to dilation (indicated by the red arrow), but doesn't go to completion and failure. The sample behavior up to this point, including the initial yielding (below 0.2 MPa axial stress) and unloading behavior, is indicative of sample constitutive response, but we argue that behavior above the black line at ~ 0.96 MPa is probably dominated by tensile yielding of the jacketing material.

3.6.3 Axisymmetric Compression Triaxial Tests

Kayenta results for multiple triaxial tests with constant lateral stresses ranging from 5 to 100 MPa are shown in **Figures 18** and **19**. Results are shown using local parameters for tests 4 and 6 (A and B in **Figures 18** and **19**) and global parameters are shown for tests 11-2 and 27 (C and D respectively in **Figures 18** and **19**). In general the results are satisfactory; Kayenta reproduces the loading paths, yielding, and failure observed in the experiments. In the case of test 27, there is a good match between *Kayenta* results and observed behavior in the pressure-volumetric strain relationships (**Figure 19D**); the axial stress-strain results in **Figure 18D** do not exhibit a good match. Sample preparation for test 27 involved tamping which produced an initial anisotropy evident in the experimental behavior (this is especially clear in the hydrostatic loading portions; unlike the other experiments there is a large difference in the lateral and axial strains during this portion, seen in the less-than 125 MPa portion in **Figure 18D**). The assumptions of isotropy in *Kayenta* preclude a good material description in this case, although it is interesting that the volume strain path exhibits a good match to test results (**Figure 19D**), and test 27 plastic volume strain behavior follows a similar path to the other tests (**Figure 15A**). The volume strain "turn-around", following a change from compaction-dominant to dilational dominant just prior to failure, is well captured for all four tests as observed in **Figure 19**.

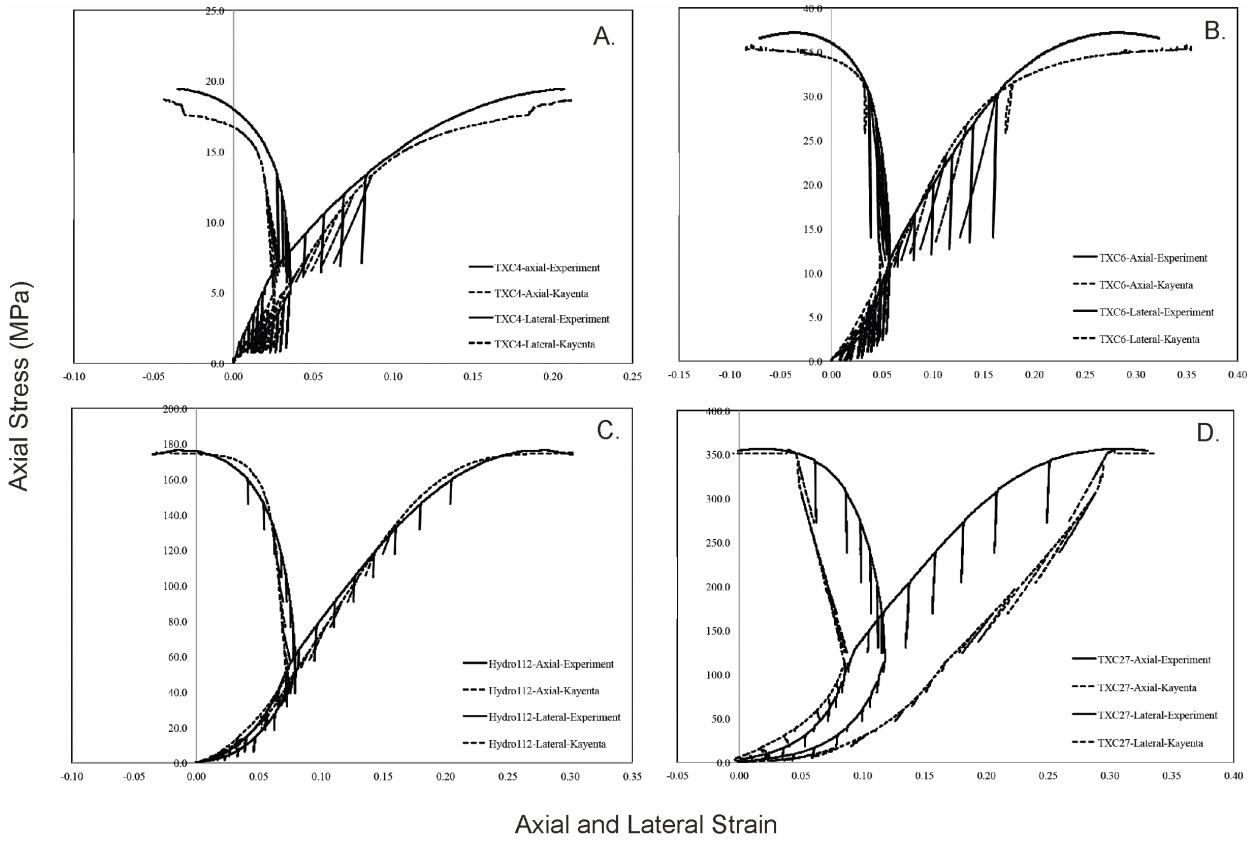

Figure 18 Triaxial test results shown as axial stress versus strain for test 4 (A), test 6 (B), test 11-2 (C) and test 27 (D) along with *Kayenta* modeling comparisons. Following an initial hydrostatic loading, the branching curves on the right hand side are axial strains and the ones on the left hand side are lateral strains.

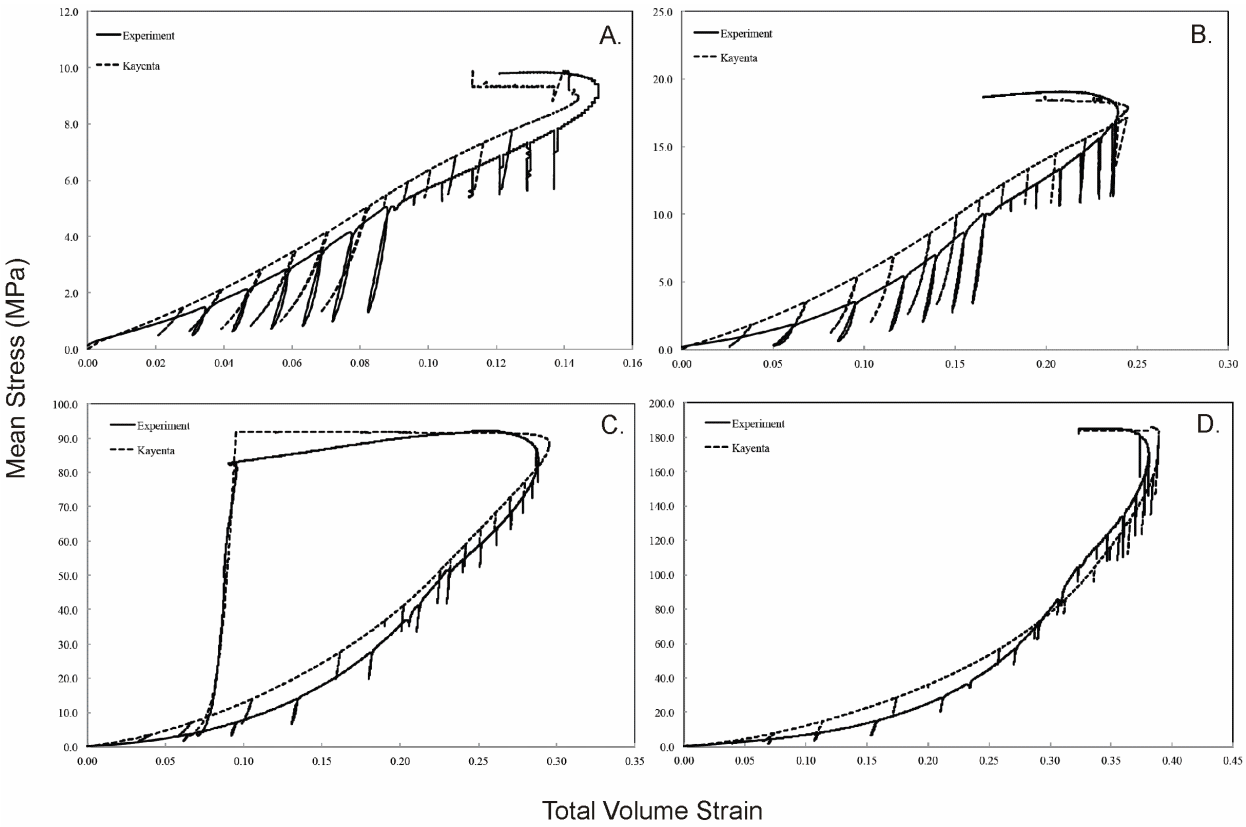

Figure 19. Mean stress-volume strain behavior for triaxial tests including test 4 (A), test 6 (B), test 11-2 (C), and test 27 (D).

3.6.4 Model Prediction Along Uniaxial Strain Loading Path

Figure shows the results of uniaxial test modeling by *Kayenta*. Since this test was in the lower stress region, local *P* parameters defined in Table were used in this test. Unfortunately, *Kayenta* over-predicts the volumetric strain of the material below 10 MPa and under-predicts it above 10 MPa.

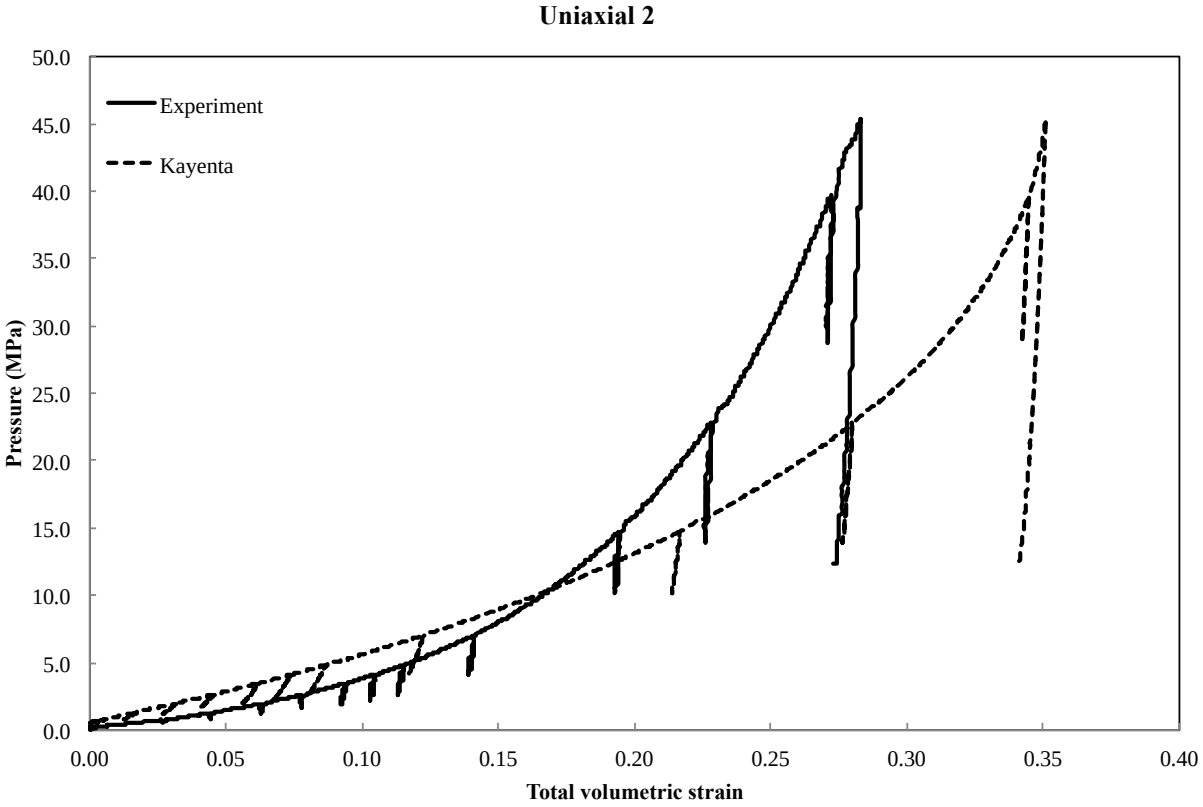

Figure 20. Uniaxial test result modeling by *Kayenta*.

4. Conclusions and Recommendations

We can make the following conclusions and recommendations about using the parameterized *Kayenta* data set, and soil constitutive modeling in general:

- Kayenta generates good descriptions of soil behavior over a broad range in mean and differential stresses. Required physics to model soil elasto-plastic constitutive behavior include: nonlinear elasticity with I_1 or mean stress-dependent elastic moduli; non-associative plasticity; kinematic and isotropic hardening; an I_1-dependent failure surface. Surprisingly, no discernable modulus degradation was observed over the entire mean stress range of the testing.
- Comparison of "tamped" soil sample and "gravity pour" sample behavior shows that plastic volume strain evolution interestingly seems to be independent of sample preparation techniques but is very sensitive to the estimates of initial pore volume or porosity. Careful measurement of the initial sample pore volume is necessary to ensure the best possible *Kayenta* model.
- Tamped sample preparation results in an anisotropic fabric that is not well captured by the isotropic assumptions of the current *Kayenta* model. Nevertheless, plastic volume strain behavior and failure under axisymmetric compression appear to be independent of initial preparation type.

- The second order polynomial function used in the Gurson "crush-curve" analysis of the soil samples could be improved, and caution is advised in using *Kayenta* outside of the mean stress range of the testing used for parameterization. This is probably the biggest source of discrepancy between *Kayenta* and experimental results, including the validation shown in **Figure 20**. We show that a fourth-order polynomial describes experimental results to an excellent degree, but some sort of exponential function would also likely provide a better description than the function currently in use.

5. References

Brannon, R.M., Fossum, A.F., and Strack, O.E., 2009. *Kayenta*: Theory and User's Guide. Sandia National Laboratories, SAND Report SAND2009-2282, Albuquerque, New Mexico, 186 p.

Dewers, T., Newell, P., Broome, S., Heath, J., and Bauer, S., 2014. Geomechanical behavior of Cambrian Mount Simon Sandstone reservoir lithofacies, Iowa Shelf, USA. International Journal of Greenhouse Gas Control 21, 33-48.

Fossum, A.F. and Fredrich, J.T., 2000. Cap plasticity models and compactive and dilatant pre-failure deformation. Proc. 4th North American Rock Mechanics Symposium, NARMS 2000, Seattle, WA, July 3 – August 1, 1169-1176.

Foster, C.D., Regueiro, R.A., Borja, R.I., and Fossum, A.F., 2005. Implicit integration of a three-invariant, single-surface, isotropic/kinematic hardening, cap plasticity model for geomaterials. Comput. Methods Appl. Mech. Eng. 194, 5109 − 5138.

Gajo, A., and Muir Wood, D., 1999. A kinematic hardening constitutive model for sands: The multiaxial formulation. Int. J. Num. Anal. Methods in Geomech. 23, 925-965, doi: 10.1002/(SICI)1096-9853.

Gurson, A.L., 1977. Continuum theory of ductile rupture by void nucleation and growth: Part I – Yield criteria and flow rules for porous ductile media. J. Eng. Mater. Technol. 99(1), 2-16, doi:10.1115/1.3443401.

Hueckel, T., Tutumluer, E., and Pellegrini, R., 1992. A note on non-linear elasticity of isotropic overconsolidated clays. International Journal for Numerical and Analytical Methods in Geomechanics 16, 603-618.

Jeske, T., and Lefik, M., 2005, Dependence of dynamic moduli on the mean stress and void ratio in the light of experimental data. Studia Geotechnica Mechanica 27, 91-100.

Kaselow, A. and Shapiro, S.A., 2004. Stress sensitivity of elastic moduli and electrical resistivity in porous rocks. Journal of Geophysics and Engineering 1, 1-11, doi:10.1088/1742-2132/1/1/001.

Pelessone, D., 1989. A modified formulation of the cap model. Gulf Atomics Report GAC19579, prepared for the Defense Nuclear Agency under Contract DNA-001086-C-0277.

Santos, J.A., Gomes Correia, A., Modaressi, A., Lopez-Caballero, F., and Carrilho-Gomes, R., 2003, Validation of an elastoplastic model to predict secant shear modulus of natural soils by experimental results. In "Deformation Characteristics of Geomaterials" (H. Di Benedetto, H. Geoffroy, T. Doanh, and C. Sauzeat, eds), Taylor and Francis, New York. P 1057- 1062, DOI: 10.1201/NOE9058096043.ch134.

Schwer, L.E., and Murry, Y.D., 1994. A three-invariant smooth cap model with mixed hardening. Int. J. Num. Anal. Methods. In Geomech. 18(10), 657-688, doi:10.1002/nag.1610181002.

Appendix A. Test Matrix and Raw Experimental Data

Table A-1: Proposed test matrix showing sample number, target density, confining pressure, order of test execution, preparation method, and initial and final sample weight and dimensions.

Sample Number	Target Density (g/cc)	Confining Pressure (psi)	Order of Test Execution	Preparation	Initial				Final					Comments
					Mass	Length	Volume	Density	Mass	Length	Diam	Volume	Density	
					grams	cm	cc	(g/cc)	grams	cm	cm	cc	(g/cc)	
01-1	1.1	0	3	Gravity pour	285.4	10.4	211	1.35						Test in vessel w/o fluid; vent to atm
02-1	1.1	0	3	Gravity pour	290.9	10.4	211	1.38						Uniaxial Strain test
03-1	1.1	725	3	Gravity pour	289.3	10.4	211	1.37						
04-1	1.1	725	3	Gravity pour	293.1	10.4	211	1.39						Sample compacted axially ≈ 0.35" during vessel assembly.
05-1	1.1	1450	3	Gravity pour	267.0	10.2	206	1.30						Sample compacted axially ≈ 0.1" during vessel assembly.
06-1	1.1	1450	3	Gravity pour	288.9	10.4	211	1.37						
07	1.1	2900	3	Gravity pour										
08	1.1	2900	3	Gravity pour										
09	1.1	4350	3	Gravity pour										
10	1.1	4350	3	Gravity pour										
11-1	1.1	7250	1	Gravity pour	296.0	10.9	221	1.34						Jacket leaked at 7100 psi; Retest sample
11-2	1.1	7250	1	Gravity pour	329.8	10.4	211	1.56						Successful test; Barrel shaped
12	1.1	7250	2	Gravity pour										
13-1	1.1	14500	1	Gravity pour	290.0	10.4	211	1.37	283.6	7.7	5.15	160.4	1.77	Reached frame cap.(>210 kip), unusual lat disp
14	1.1	14500	2	Gravity pour										
15	1.4	0	3	Tamp in lifts										
16	1.4	0	3	Tamp in lifts										
17	1.4	725	3	Tamp in lifts										
18	1.4	725	3	Tamp in lifts										
19	1.4	1450	3	Tamp in lifts										
20	1.4	1450	3	Tamp in lifts										
21	1.4	2900	3	Tamp in lifts										
22	1.4	2900	3	Tamp in lifts										
23	1.4	4350	3	Tamp in lifts										
24	1.4	4350	3	Tamp in lifts										
25-1,2,3	1.4	7250	1	Tamp in lifts	345.6	10.7	216	1.60						INT LC max'd, retested same sample, leaked
25-4	1.4	7250	1	Tamp in lifts	367.6	10.2	207	1.77						Failure in axial LVDT's . Unloaded test w/o completion
25-5	1.4	7250	1	Tamp in lifts	338.4	10.3	208	1.62	335.0	7.2	5.59	176.3	1.90	Successful test
26	1.4	7250	2	Tamp in lifts										
27-1	1.4	14500	1	Tamp in lifts	333.1	10.5	214	1.56	329.6	7.6	5.08	155.0	2.13	Successful test, reached frame cap.(>210 kip)
28	1.4	14500	2	Tamp in lifts										

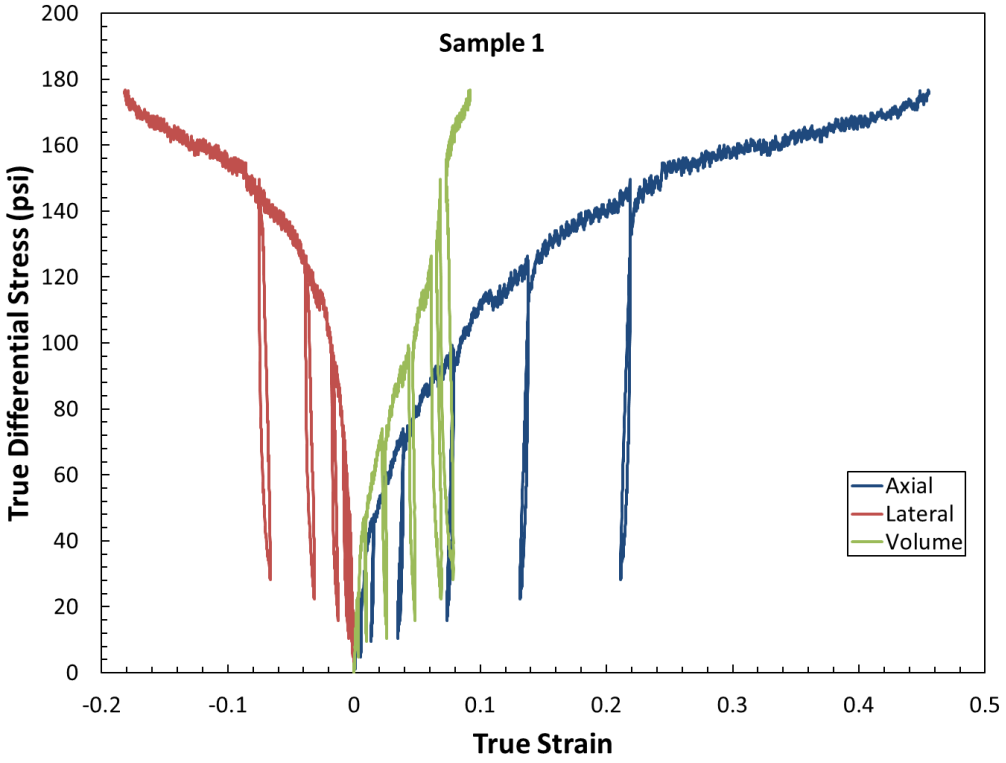

Figure A1: True differential stress versus true strain for sample 1 (unconfined).

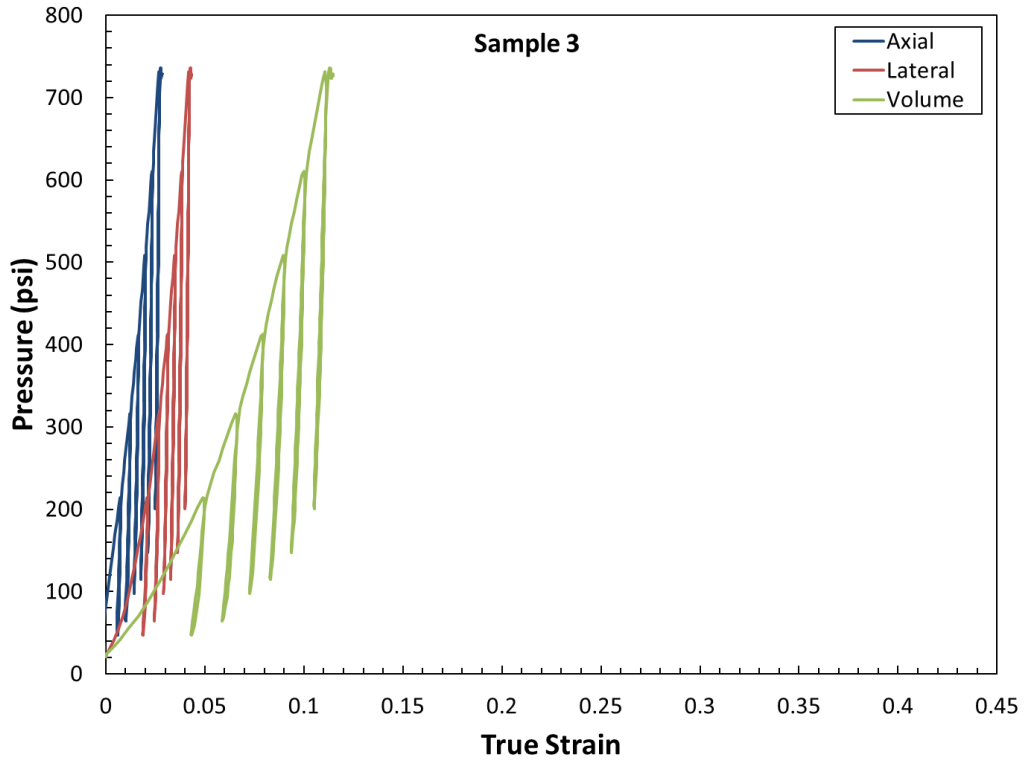

Figure A2: Pressure versus true strain for sample 3.

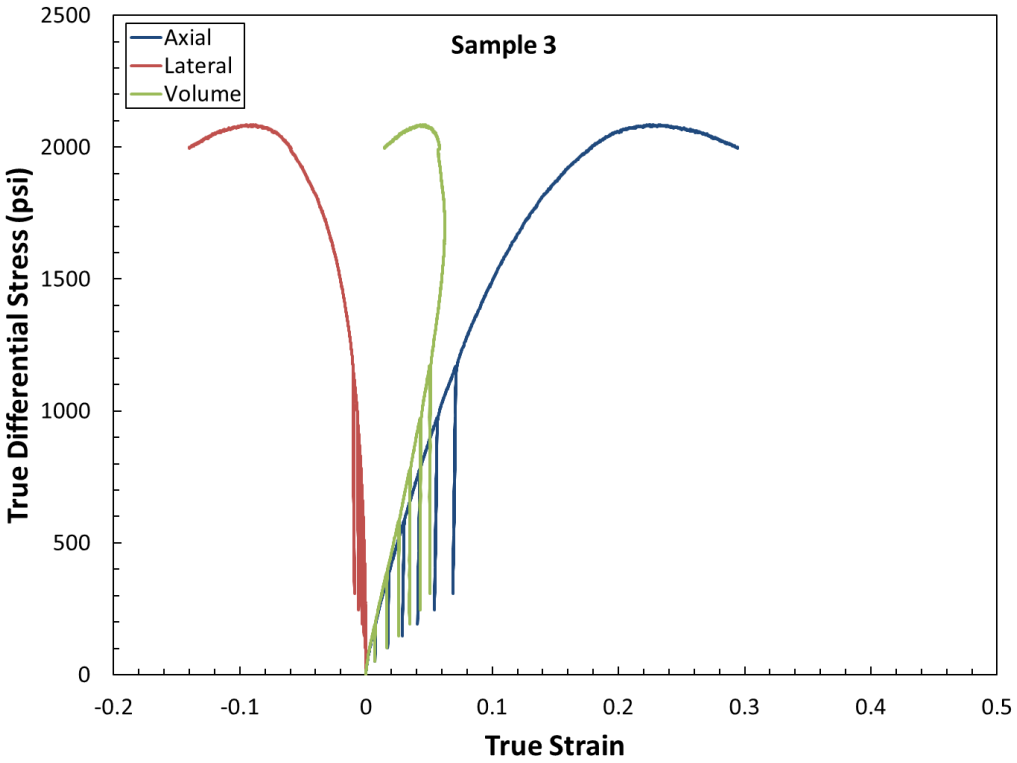

Figure A3: True differential stress versus true strain for sample 3.

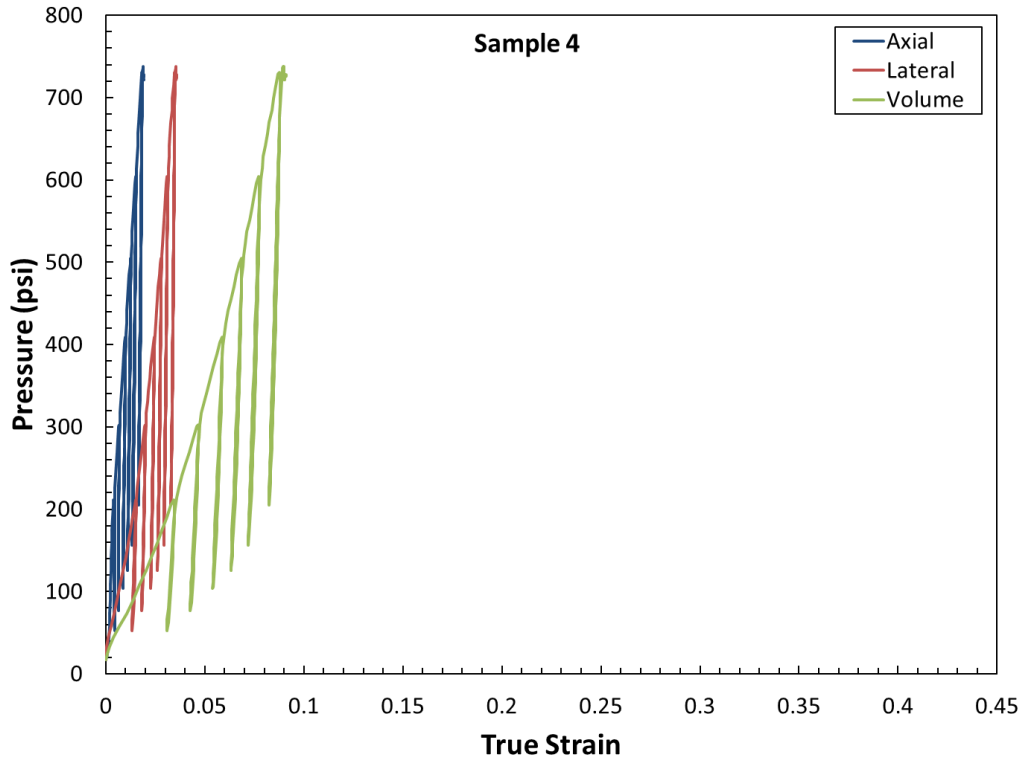

Figure A4: Pressure versus true strain for sample 4.

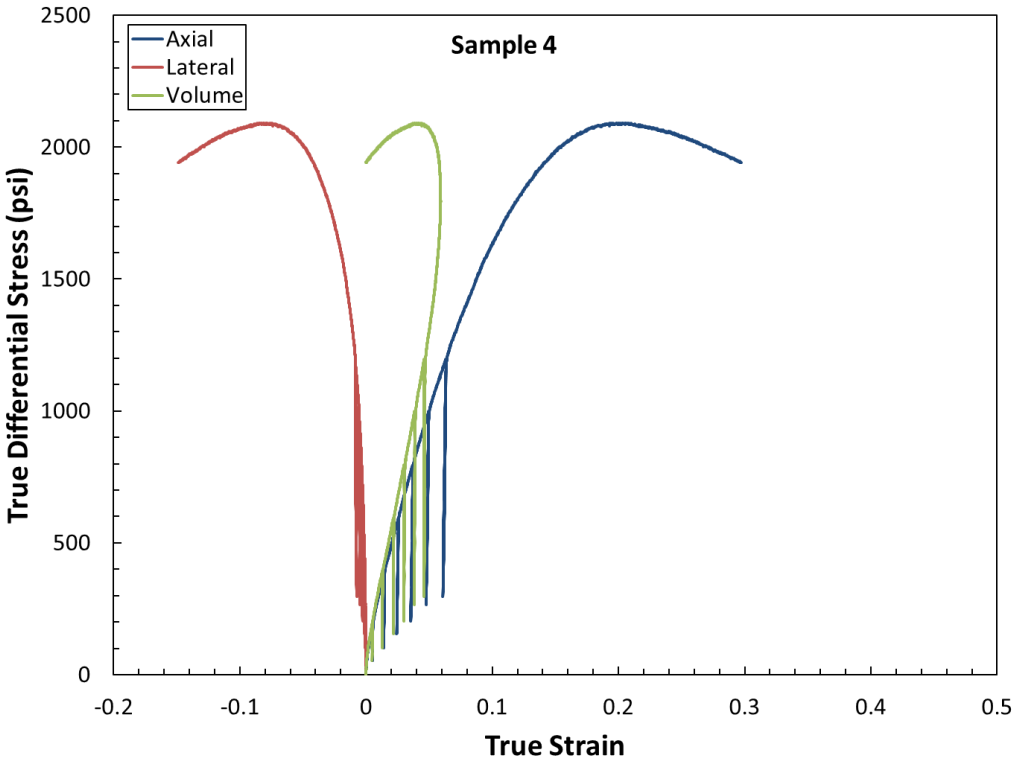

Figure A5: True differential stress versus true strain for sample 4.

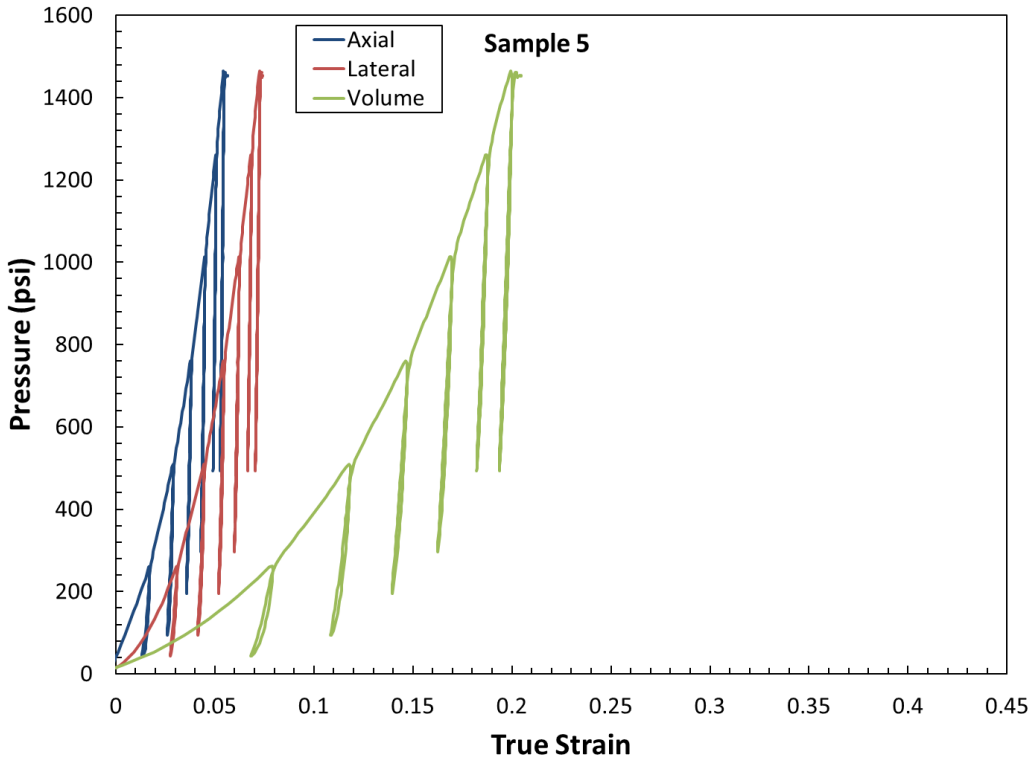

Figure A6: Pressure versus true strain for sample 5.

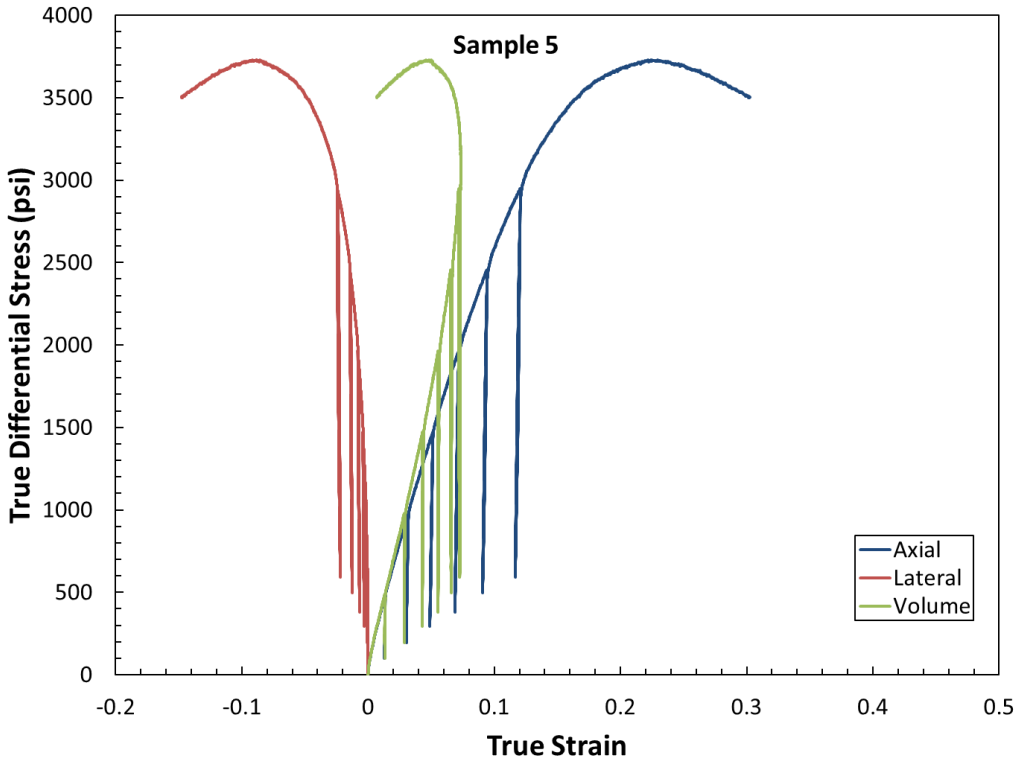

Figure A7: True differential stress versus true strain for sample 5.

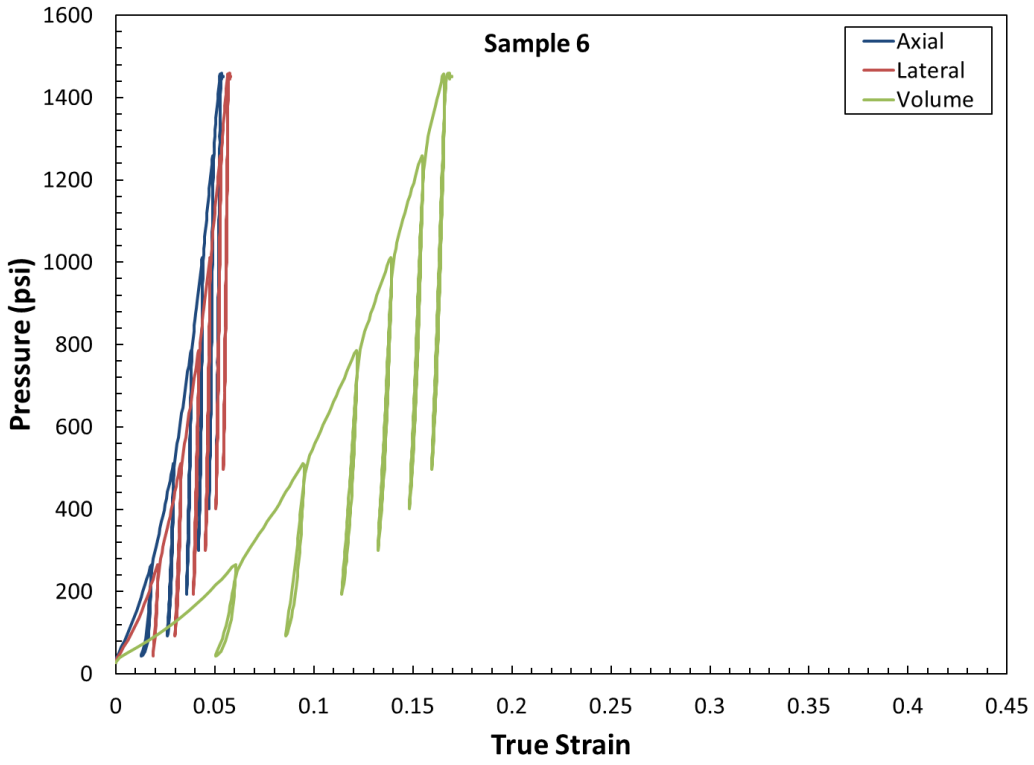

.

Figure A8: Pressure versus true strain for sample 6.

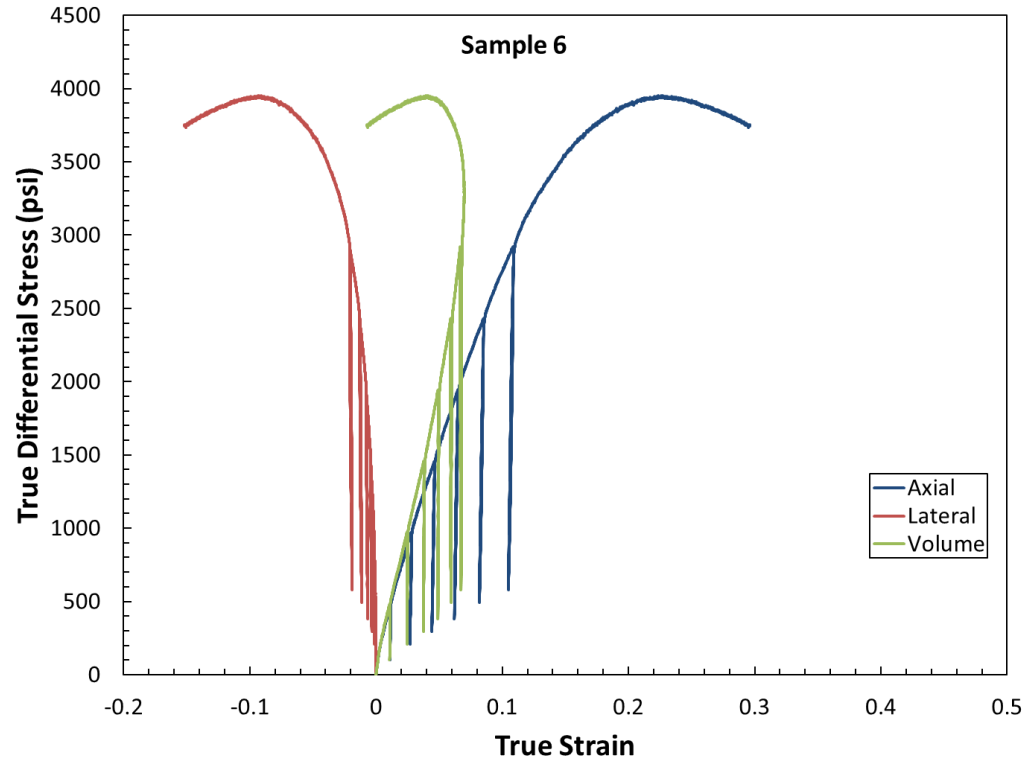

Figure A9: True differential stress versus true strain for sample 6.

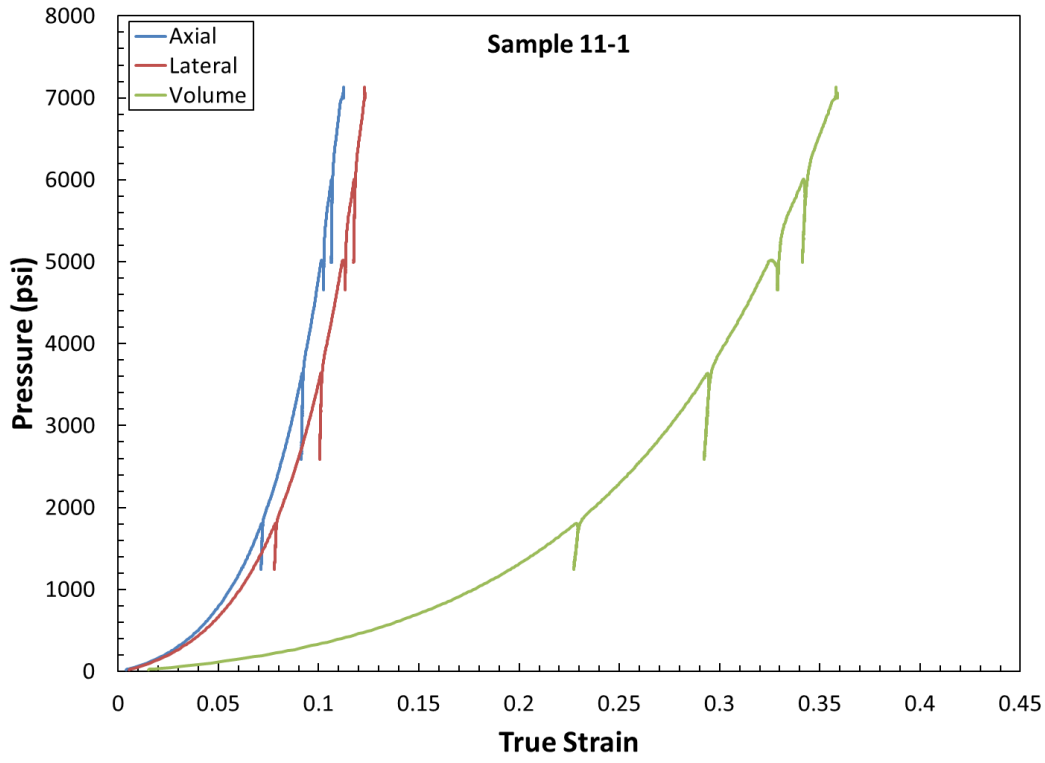

Figure A10: Pressure versus true strain for sample 11-1.

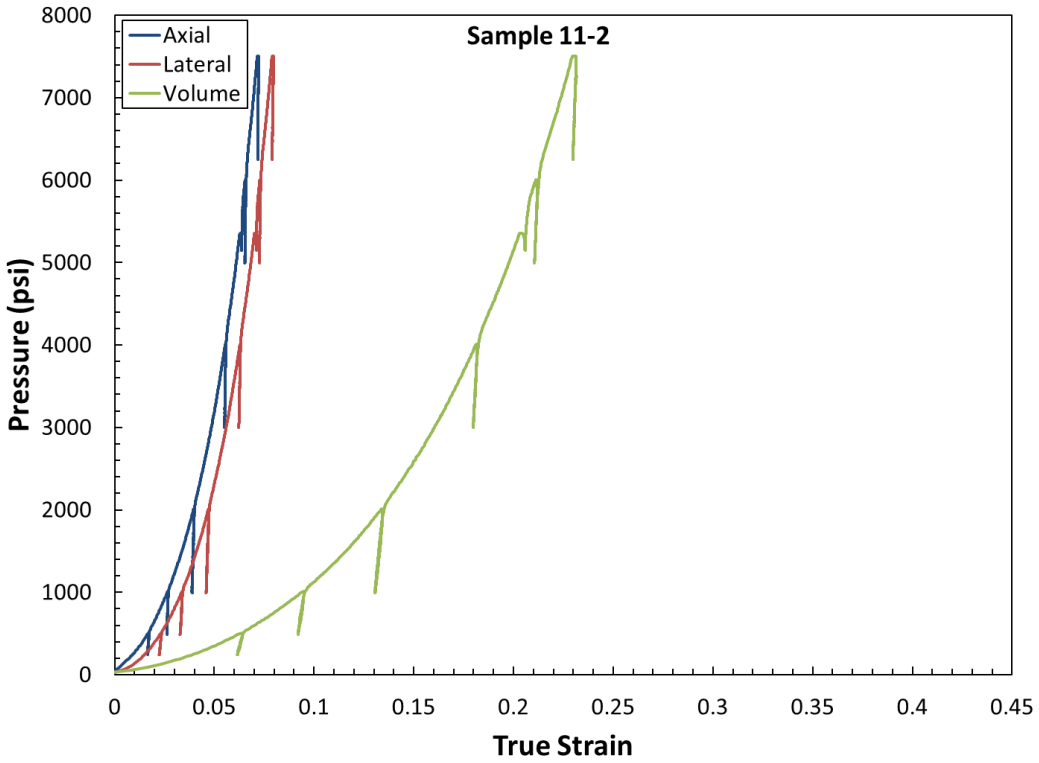

Figure A11: Pressure versus true strain for sample 11-2.

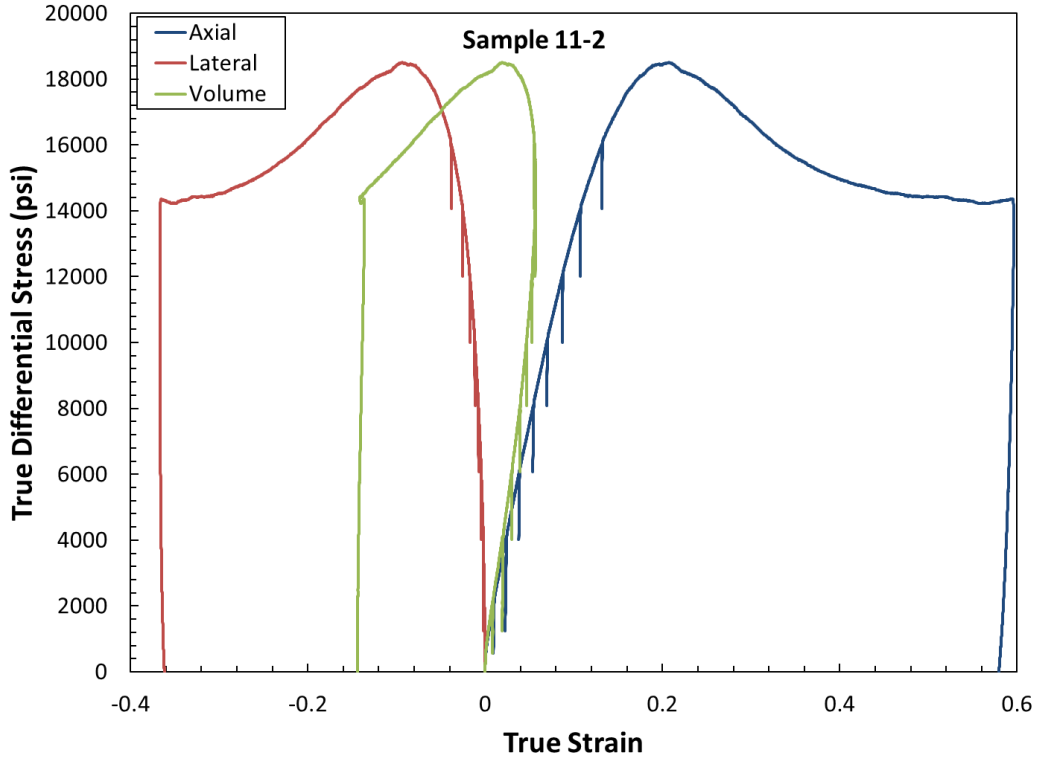

Figure A12: True differential stress versus true strain for sample 11-2 (x-axis scaling not consistent with other plots in order to show post peak behavior captured during this test).

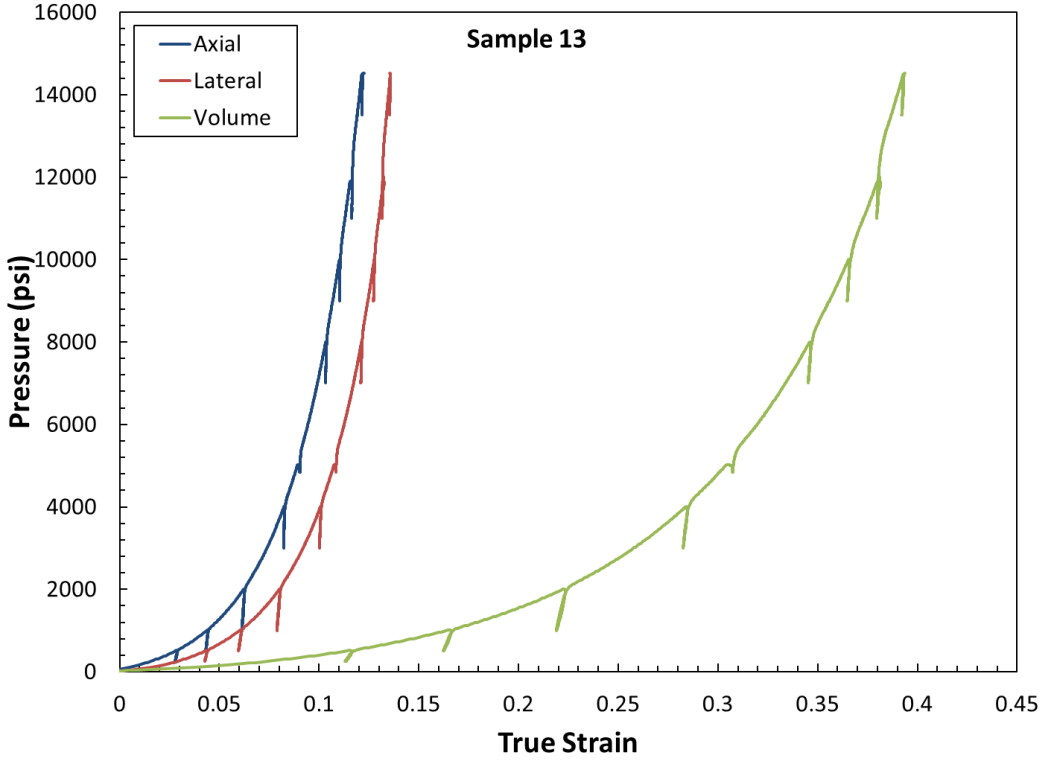

Figure A13: Pressure versus true strain for sample 13.

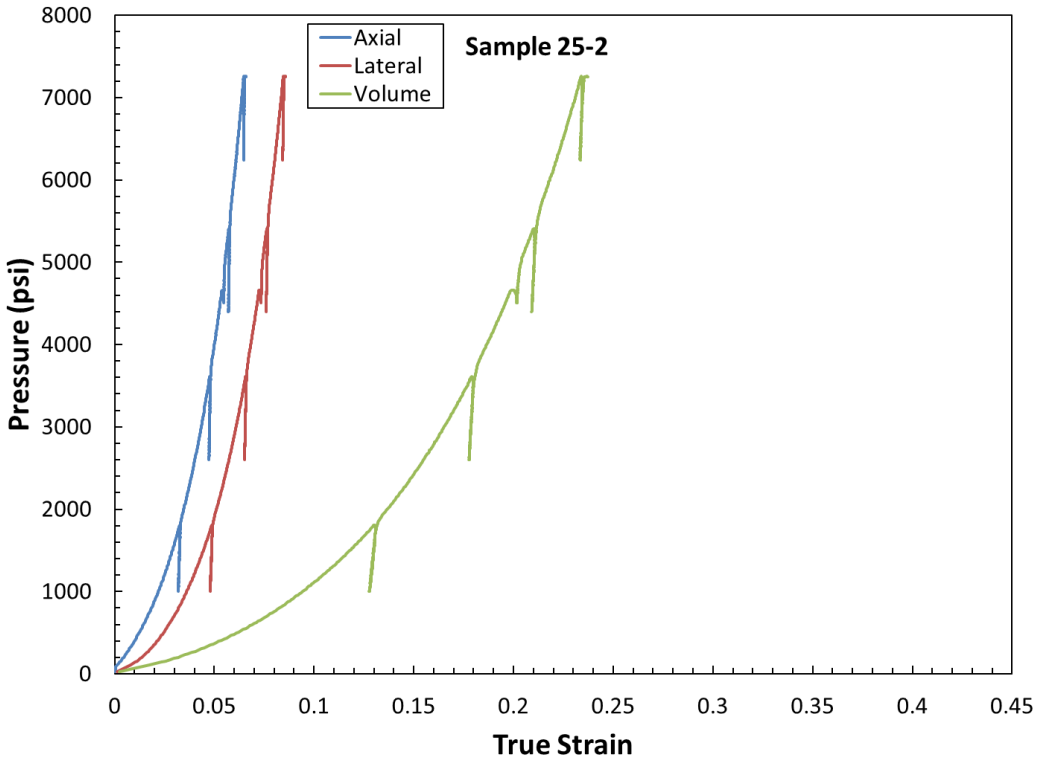

Figure A14: Pressure versus true strain for sample 25-2.

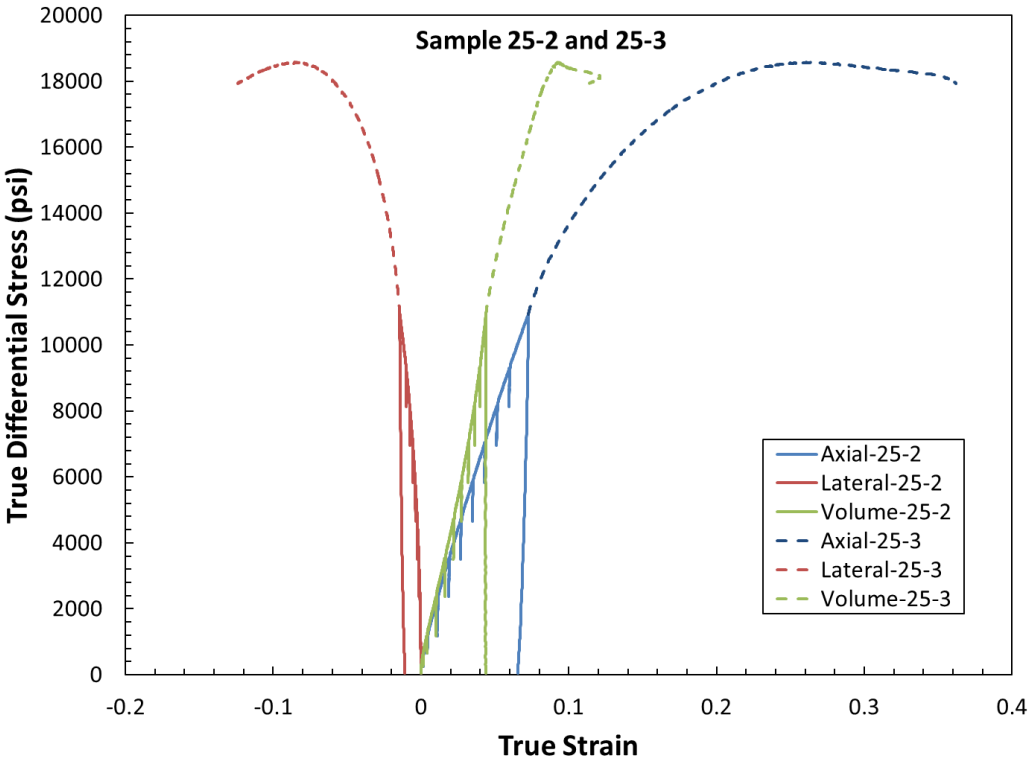

Figure A15: True differential stress versus true strain for sample 25-2,3.

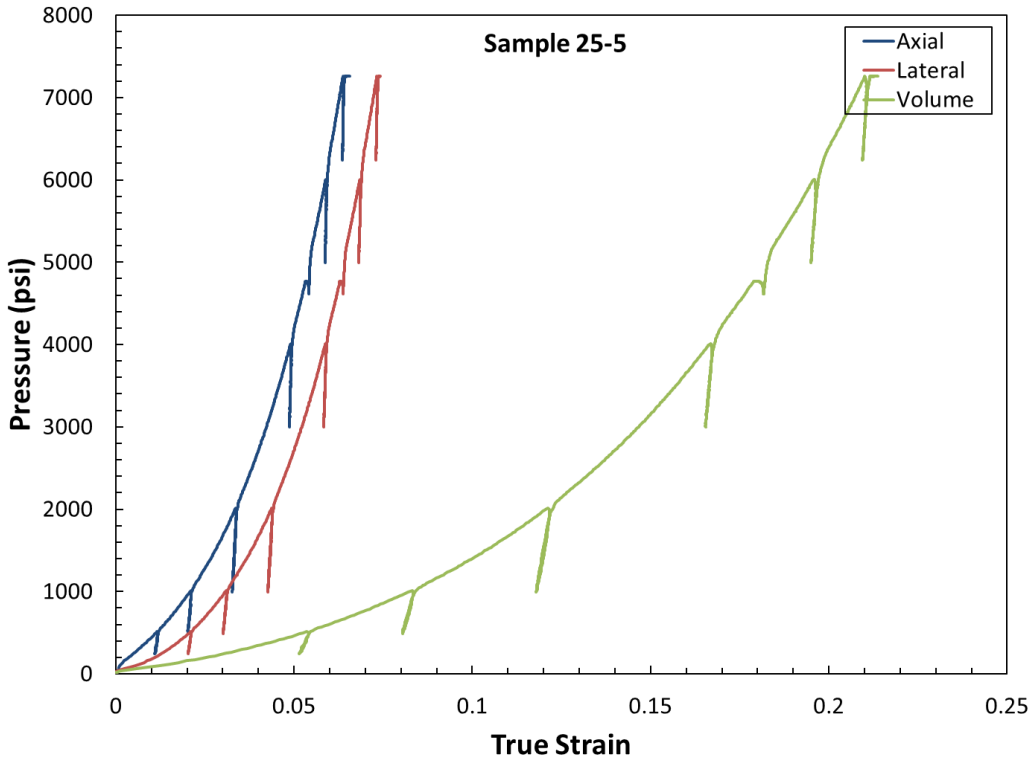

Figure A16: Pressure versus true strain for sample 25-5.

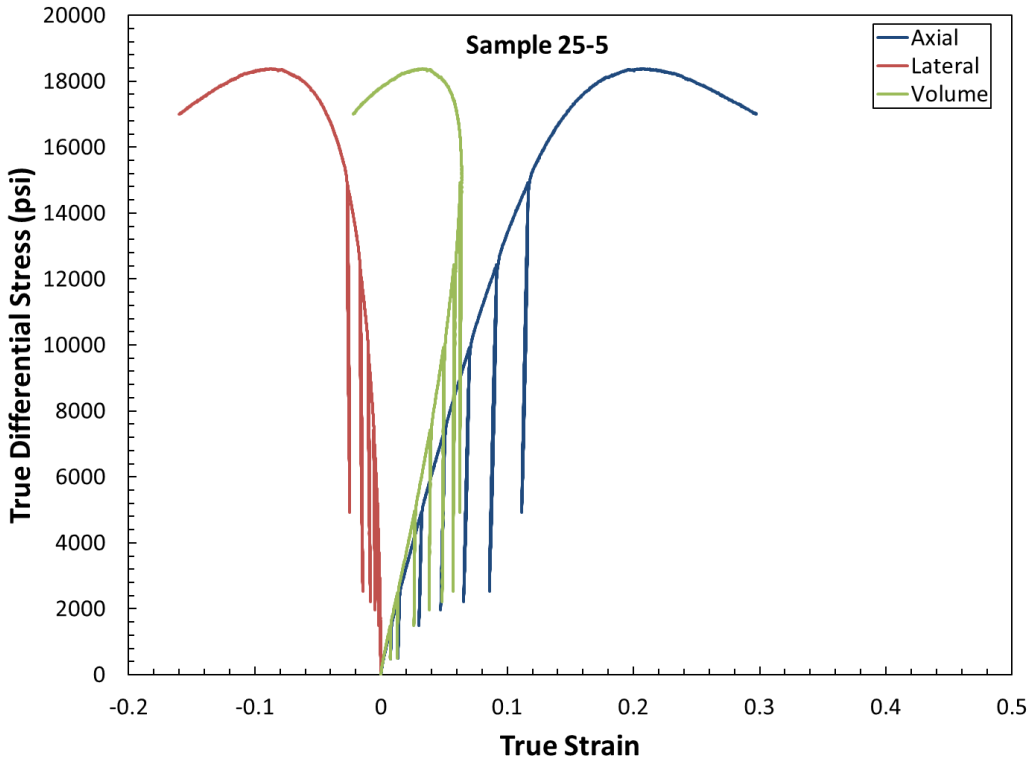

Figure A17: True differential stress versus true strain for sample 25-5.

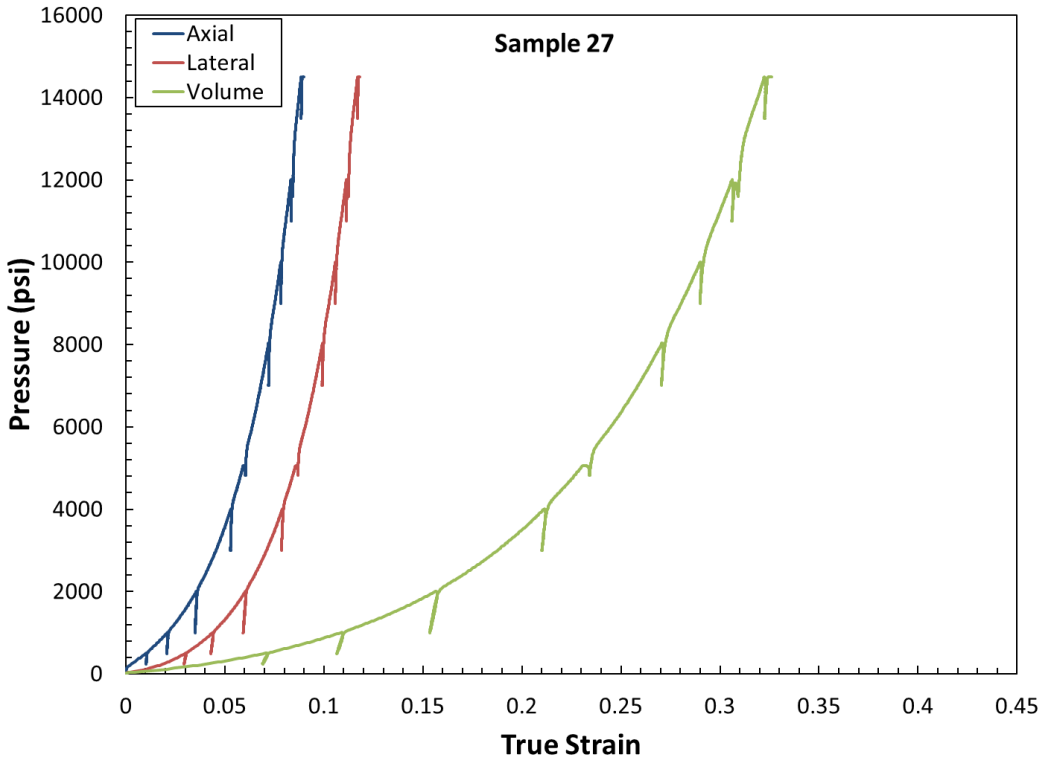

Figure A18: Pressure versus true strain for sample 27.

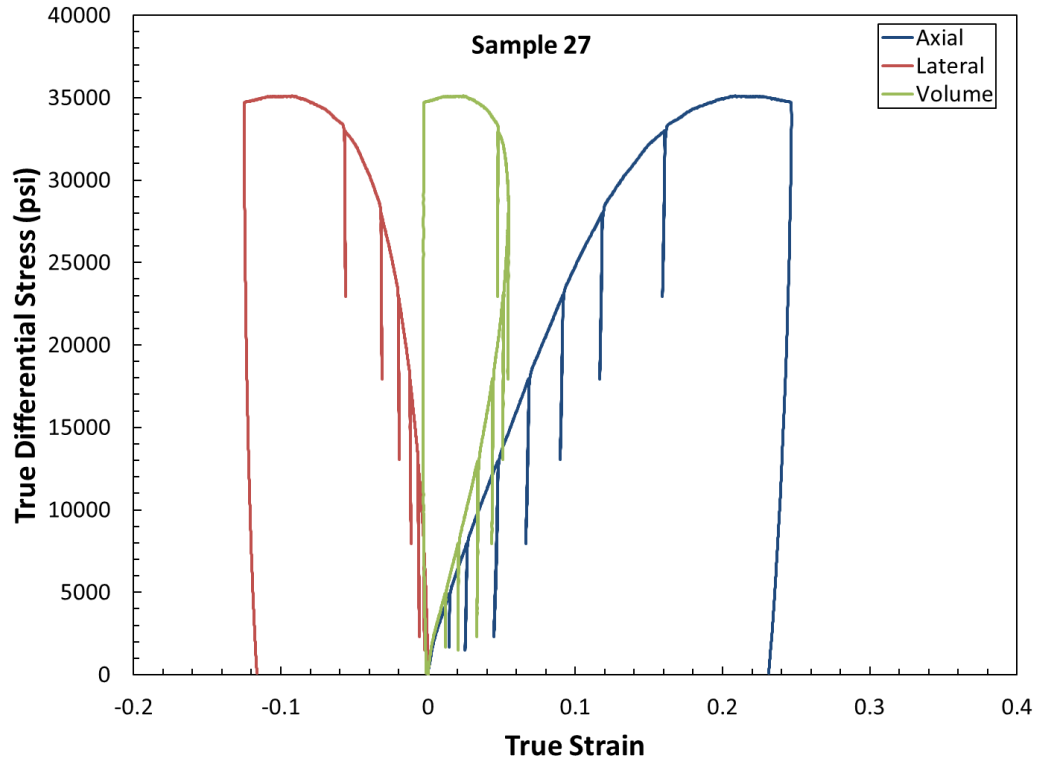

Figure A19: True differential stress versus true strain for sample 27.

Appendix B. Summary of Kayenta Parameters

Below are two sample input files in the xml format, used in MatModLab driver for Kayenta material model. The first one has the local parameters used in Hydro11-1, TXC4 and TXC6 and the second one has the global parameters used in Hydro11-2 and TXC27.

Local:

```
<?xml version="1.0" ?>
<MMLSpec>
  <Physics>
    <Material model="kayenta">
      <B0> 1148.0E+06</B0>
      <B1> 9.80E-09</B1>
      <B2> 0.93</B2>
      <B3> 0.012E-6</B3>
      <G0> 300e6</G0>
      <G1> 2.00E-8</G1>
      <G2> 0.9</G2>
      <G3> 0.012E-6</G3>
      <A1> 0.95E+06</A1>
      <A2> 0.011105E-06</A2>
      <A3> 0.585145E+06</A3>
      <A4> 0.261969</A4>
      <P0> -0.78557E+06</P0>
      <P1> 8.9E-9</P1>
      <P2> -3.0E-17</P2>
      <P3> 0.571</P3>
      <CR> 1.3400</CR>
      <RN> 0.340E+06</RN>
      <J3TYPE> 3.00</J3TYPE>
      <EOSID> 6.00</EOSID>
    </Material>
    <Path type="prdef" ndumps="all">
```

Global:

```
<?xml version="1.0" ?>
<MMLSpec>

  <Physics>
    <Material model="kayenta">
      <B0> 1148.00E+06</B0>
      <B1> 9.80E-09</B1>
      <B2> 0.93</B2>
      <B3> 0.012E-6</B3>
```

```
  <G0> 300e6</G0>
  <G1> 2.00E-8</G1>
  <G2> 0.9</G2>
  <G3> 0.012E-6</G3>
  <A1> 0.95E+06</A1>
  <A2> 0.011105E-06</A2>
  <A3> 0.585145E+06</A3>
  <A4> 0.261969</A4>
  <P0> -0.78557E+06</P0>
  <P1> 0.00536E-6</P1>
  <P2> -0.0000067E-12</P2>
  <P3> 0.371064</P3>
  <CR> 1.3400</CR>
  <RN> 0.340E+06</RN>
  <HC> 8.0E+02</HC>
  <CRPF> 1.629</CRPF>
  <A2PF> 0.011E-08</A2PF>
  <A4PF> 0.2423</A4PF>
  <J3TYPE> 3.00</J3TYPE>
  <EOSID> 6.00</EOSID>
</Material>
<Path type="prdef" ndumps="all">
```

Appendix C. Soil Analysis Report from Daniel B. Stephens & Associates, Inc.

Laboratory Report for
Sandia National Laboratories

San Ysidro Alluvium Sample

July 3, 2014

Daniel B. Stephens & Associates, Inc.
4400 Alameda Blvd. NE, Suite C • Albuquerque, New Mexico 87113

July 3, 2014

Thomas Dewers
Geomechanics
Sandia National Laboratories
PO Box 5800 MS0751
Albuquerque, NM 87185-0751
(505) 845-0631

Re: DBS&A Laboratory Report for the Sandia National Laboratories, San Ysidro Alluvium Sample

Dear Mr. Dewers:

Enclosed is the report for the Sandia National Laboratories, San Ysidro Alluvium sample. Please review this report and provide any comments as samples will be held for a maximum of 30 days. After 30 days samples will be returned or disposed of in an appropriate manner.

All testing results were evaluated subjectively for consistency and reasonableness, and the results appear to be reasonably representative of the material tested. However, DBS&A does not assume any responsibility for interpretations or analyses based on the data enclosed, nor can we guarantee that these data are fully representative of the undisturbed materials at the field site. We recommend that careful evaluation of these laboratory results be made for your particular application.

The testing utilized to generate the enclosed report employs methods that are standard for the industry. The results do not constitute a professional opinion by DBS&A, nor can the results affect any professional or expert opinions rendered with respect thereto by DBS&A. You have acknowledged that all the testing undertaken by us, and the report provided, constitutes mere test results using standardized methods, and cannot be used to disqualify DBS&A from rendering any professional or expert opinion, having waived any claim of conflict of interest by DBS&A.

We are pleased to provide this service to Sandia National Laboratories and look forward to future laboratory testing on other projects. If you have any questions about the enclosed data, please do not hesitate to call.

Sincerely,

DANIEL B. STEPHENS & ASSOCIATES, INC.
SOIL TESTING & RESEARCH LABORATORY

Crystal Krous

Crystal Krous
Quality Analyst; for Joleen Hines

Enclosure

Daniel B. Stephens & Associates, Inc.
Soil Testing & Research Laboratory
4400 Alameda Blvd. NE, Suite C
Albuquerque, NM 87113
505-889-7752
FAX 505-889-0258

Summaries

Summary of Tests Performed

Laboratory Sample Number	Initial Soil Properties[1]			Saturated Hydraulic Conductivity[2]			Moisture Characteristics[3]								Particle Size[4]			Specific Gravity[5]		Air Perm-eability	Atterberg Limits	Proctor Compaction
	G	VM	VD	CH	FH	FW	HC	PP	FP	DPP	RH	EP	WHC	K_{unsat}	DS	WS	H	F	C			
San Ysidro Alluvium																X	X				X	

[1] G = Gravimetric Moisture Content, VM = Volume Measurement Method, VD = Volume Displacement Method
[2] CH = Constant Head Rigid Wall, FH = Falling Head Rigid Wall, FW = Falling Head Rising Tail Flexible Wall
[3] HC = Hanging Column, PP = Pressure Plate, FP = Filter Paper, DPP = Dew Point Potentiometer, RH = Relative Humidity Box, EP = Effective Porosity, WHC = Water Holding Capacity, Kunsat = Calculated Unsaturated Hydraulic Conductivity
[4] DS = Dry Sieve, WS = Wet Sieve, H = Hydrometer
[5] F = Fine (<4.75mm), C = Coarse (>4.75mm)

4

Notes

Sample Receipt:
One sample was hand delivered, in a 1/2 full 5-gallon bucket sealed with a lid, on June 25, 2014.

Sample Preparation and Testing Notes:
The sample was subjected to particle size analysis and Atterberg limits testing.

General Notes:
An assumed specific gravity value of 2.65 was used to perform the particle diameter calculations in the hydrometer portion of the particle size analysis.

Summary of Particle Size Characteristics

Sample Number	d_{10} (mm)	d_{50} (mm)	d_{60} (mm)	C_u	C_c	Method	ASTM Classification	USDA Classification	
San Ysidro Alluvium	0.00088	0.11	0.19	216	5.4	WS/H	Silty sand (SM)	Sandy Loam	(Est)

d_{50} = Median particle diameter

Est = Reported values for d_{10}, C_u, C_c, and soil classification are estimates, since extrapolation was required to obtain the d_{10} diameter

$C_u = \frac{d_{60}}{d_{10}}$

$C_c = \frac{(d_{30})^2}{(d_{10})(d_{60})}$

DS = Dry sieve

H = Hydrometer

WS = Wet sieve

† Greater than 10% of sample is coarse material

6

Percent Gravel, Sand, Silt and Clay*

Sample Number	% Gravel (>4.75mm)	% Sand (<4.75mm, >0.075mm)	% Silt (<0.075mm, >0.002mm)	% Clay (<0.002mm)
San Ysidro Alluvium	0.0	56.9	30.2	13.0

*USCS classification does not classify clay fraction based on particle size. USDA definition of clay (<0.002mm) used in this table.

7

Summary of Atterberg Tests

Sample Number	Liquid Limit	Plastic Limit	Plasticity Index	Classification
San Ysidro Alluvium	---	---	---	ML

--- = Soil requires visual-manual classification due to non-plasticity

Particle Size Analysis

9

Summary of Particle Size Characteristics

Sample Number	d_{10} (mm)	d_{50} (mm)	d_{60} (mm)	C_u	C_c	Method	ASTM Classification	USDA Classification	
San Ysidro Alluvium	0.00088	0.11	0.19	216	5.4	WS/H	Silty sand (SM)	Sandy Loam	(Est)

d_{50} = Median particle diameter

Est = Reported values for d_{10}, C_u, C_c, and soil classification are estimates, since extrapolation was required to obtain the d_{10} diameter

$$C_u = \frac{d_{60}}{d_{10}}$$

$$C_c = \frac{(d_{30})^2}{(d_{10})(d_{60})}$$

DS = Dry sieve

H = Hydrometer

WS = Wet sieve

† Greater than 10% of sample is coarse material

10

Percent Gravel, Sand, Silt and Clay*

Sample Number	% Gravel (>4.75mm)	% Sand (<4.75mm, >0.075mm)	% Silt (<0.075mm, >0.002mm)	% Clay (<0.002mm)
San Ysidro Alluvium	0.0	56.9	30.2	13.0

*USCS classification does not classify clay fraction based on particle size. USDA definition of clay (<0.002mm) used in this table.

11

Particle Size Analysis
Wet Sieve Data (#10 Split)

Job Name: Sandia National Laboratories-Geomechanics
Job Number: LB14.0128.00
Sample Number: San Ysidro Alluvium
Ring Number: NA
Depth: NA
Test Date: 3-Jul-14

Initial Dry Weight of Sample (g): 297.30
Weight Passing #10 (g): 284.95
Weight Retained #10 (g): 12.35
Weight of Hydrometer Sample (g): 50.56
Calculated Weight of Sieve Sample (g): 52.75

Shape: Angular
Hardness: Soft

Test Fraction	Sieve Number	Diameter (mm)	Wt. Retained	Cum Wt. Retained	Wt. Passing	% Passing
+10						
	3"	75	0.00	0.00	297.30	100.00
	2"	50	0.00	0.00	297.30	100.00
	1.5"	38.1	0.00	0.00	297.30	100.00
	1"	25	0.00	0.00	297.30	100.00
	3/4"	19.0	0.00	0.00	297.30	100.00
	3/8"	9.5	0.00	0.00	297.30	100.00
	4	4.75	0.00	0.00	297.30	100.00
	10	2.00	12.35	12.35	284.95	95.85
-10			(Based on calculated sieve wt.)			
	20	0.85	6.01	8.20	44.55	84.45
	40	0.425	5.99	14.19	38.56	73.10
	60	0.250	4.51	18.70	34.05	64.55
	140	0.106	7.93	26.63	26.12	49.52
	200	0.075	3.36	29.99	22.76	43.15
	dry pan		0.46	30.45	22.30	
	wet pan			22.30	0.00	

d_{10} (mm): 0.00088
d_{16} (mm): 0.0028
d_{30} (mm): 0.030
d_{50} (mm): 0.11
d_{60} (mm): 0.19
d_{84} (mm): 0.83

Median Particle Diameter--d_{50} (mm): 0.11
Uniformity Coefficient, Cu--$[d_{60}/d_{10}]$ (mm): 216
Coefficient of Curvature, Cc--$[(d_{30})^2/(d_{10}*d_{60})]$ (mm): 5.4
Mean Particle Diameter--$[(d_{16}+d_{50}+d_{84})/3]$ (mm): 0.31

Note: Reported values for d_{10}, C_u, C_c, and soil classification are estimates, since extrapolation was required to obtain the d_{10} diameter

Classification of fines (visual method): ML

ASTM Soil Classification: Silty sand (SM)
USDA Soil Classification: Sandy Loam

Laboratory analysis by: S. Hanhardt
Data entered by: C. Krous
Checked by: C. Krous

12

Particle Size Analysis
Hydrometer Data

Job Name: Sandia National Laboratories-Geomechanics
Job Number: LB14.0128.00
Sample Number: San Ysidro Alluvium
Ring Number: NA
Depth: NA

Test Date: 1-Jul-14
Start Time: 9:00

Type of Water Used: DISTILLED
Reaction with H_2O_2: NA
Dispersant:* $(NaPO_3)_6$
Assumed particle density: 2.65

Initial Wt. (g): 50.56
Total Sample Wt. (g): 297.30
Wt. Passing #10 (g): 284.95

Date	Time (min)	Temp (°C)	R (g/L)	R_L (g/L)	R_{corr} (g/L)	L (cm)	D (mm)	P (%)	% Finer
1-Jul-14	1	23.1	23.0	4.9	18.1	12.5	0.04647	35.9	34.4
	2	23.1	21.0	4.9	16.1	12.9	0.03328	31.9	30.6
	5	23.1	19.5	4.9	14.6	13.1	0.02125	28.9	27.7
	15	23.1	17.5	4.9	12.6	13.4	0.01242	25.0	23.9
	30	23.1	16.0	4.9	11.1	13.7	0.00886	22.0	21.1
	60	22.8	15.0	4.9	10.1	13.8	0.00633	19.9	19.1
	120	22.7	14.0	4.9	9.1	14.0	0.00451	17.9	17.2
	250	22.6	14.0	5.0	9.0	14.0	0.00313	17.9	17.1
	482	22.9	12.0	4.9	7.1	14.3	0.00227	14.0	13.4
2-Jul-14	1498	22.5	11.0	5.0	6.0	14.5	0.00130	11.9	11.4

Comments:

* Dispersion device: mechanically operated stirring device

Laboratory analysis by: N. Candelaria
Data entered by: C. Krous
Checked by: C. Krous

13

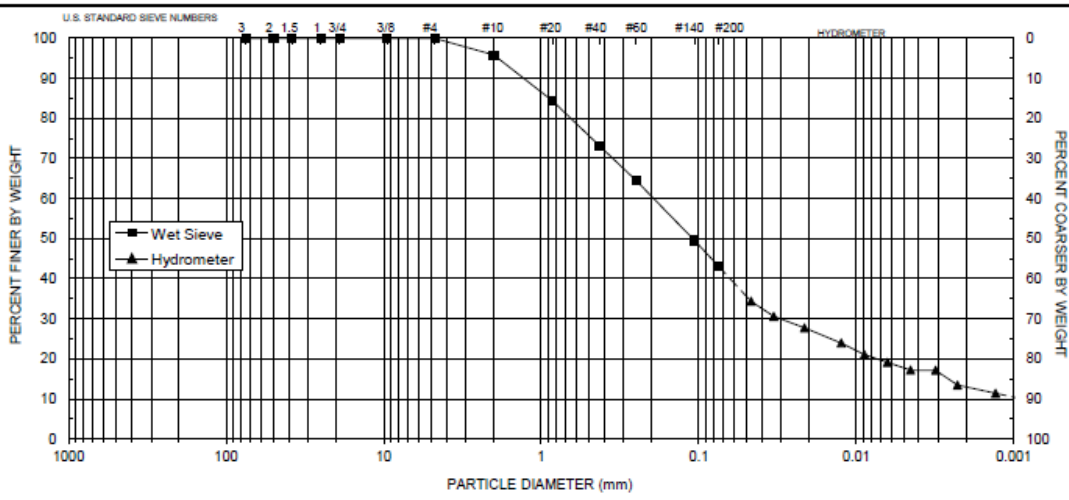

d_{10} = 0.00088	d_{30} = 0.030	d_{50} = 0.11	d_{60} = 0.19	C_u = 216	C_c = 5.4

SAMPLE NUMBER	DEPTH	ASTM CLASSIFICATION	USDA CLASSIFICATION
San Ysidro Alluvium	**NA**	**Silty sand (SM)**	**Sandy Loam**

Note: Reported values for d_{10}, C_u, C_c, and ASTM classification are estimates, since extrapolation was required to obtain the d_{10} diameter

Daniel B. Stephens & Associates, Inc.

14

Atterberg Limits/ Identification of Fines

15

Summary of Atterberg Tests

Sample Number	Liquid Limit	Plastic Limit	Plasticity Index	Classification
San Ysidro Alluvium	---	---	---	ML

--- = Soil requires visual-manual classification due to non-plasticity

Atterberg Limits

Job Name: Sandia National Laboratories-Geomechanics
Job Number: LB14.0128.00
Sample Number: San Ysidro Alluvium
Ring Number: NA
Depth: NA

Test Date: 3-Jul-14

Liquid Limit

	Trial 1	Trial 2	Trial 3
Number of drops:			
Pan number:			
Weight of pan plus moist soil (g):			
Weight of pan plus dry soil (g)			
Weight of pan (g):			
Gravimetric moisture content (% g/g):	---	---	---
Liquid Limit:	---		

Plastic Limit

	Trial 1	Trial 2
Pan number:		
Weight of pan plus moist soil (g):		
Weight of pan plus dry soil (g)		
Weight of pan (g):		
Gravimetric moisture content (% g/g):	---	---
Plastic Limit:	---	

Results

Percent of Sample Retained on #40 Sieve: See Sieve

Liquid Limit: ---
Plastic Limit: ---
Plasticity Index: ---

Classification (Visual Method): ML

Comments:

--- = Soil requires visual-manual classification due to non-plasticity
' = 1-point method requested by client

Laboratory analysis by: D. O'Dowd
Data entered by: C. Krous
Checked by: C. Krous

17

Data for Description and Identification of Fines
(Visual-Manual Procedure)

Job Name: Sandia National Laboratories-Geomechanics
Job Number: LB14.0128.00
Sample Number: San Ysidro Alluvium
Ring Number: NA
Depth: NA

Test Date: 3-Jul-14

Visual-manual classification of material passing the #40 sieve in lieu of Atterberg analysis due to non-plasticity:

Descriptive Information:

Color of Moist Sample: Dark Yellowish Brown (10 YR 3/6)
Odor: None
Moisture Condition: Moist
HCl Reaction: Strong

Preliminary Identification:

Dry Strength: None
Dilatency: Rapid
Toughness: Low
Plasticity: Non-plastic

Identification of Inorganic Fine Grained Soils:

Silt (ML)

Laboratory analysis by: D. O'Dowd
Data entered by: C. Krous
Checked by: C. Krous

18

Laboratory Tests and Methods

19

Tests and Methods

Particle Size Analysis:	ASTM D422
USCS (ASTM) Classification:	ASTM D422, ASTM D2487
USDA Classification:	ASTM D422, USDA Soil Textural Triangle
Atterberg Limits:	ASTM D4318
Visual-Manual Description:	ASTM D2488

Distribution:

1	MS-0899	Technical Library, 95036. (electronic copy)
1	MS-0612	Review & Approval Desk, 9612. (electronic copy)
1	MS-1033	Scott Broome, 06914. (electronic copy)
1	MS-1033	Greg Flint, 06914. (electronic copy)
1	MS-0751	Thomas Dewers, 06914. (electronic copy)
1	MS-0840	Pania Newell, 06914. (electronic copy)
1	MS-0840	Terry Hinnerichs, 01554. (electronic copy)
1	MS-0735	Moo Lee, 06914. (electronic copy)
1	MS-1033	Steve Bauer, 06914. (electronic copy)
1	MS-0840	Chi S. Lo, 01554. (electronic copy)
1	MS-0840	James Bean, 01554. (electronic copy)
1	MS-0836	Lubomyra N. Kmetyk, 01523. (electronic copy)
1	MS-0897	Michael K. Wong, 01446. (electronic copy)
1	MS-0840	Huei Eliot Fang, 01554. (electronic copy)


Sandia National Laboratories